December 2013

Mechanical Properties and High-temperature Performance of a Polyester Resin Modified Using FGD Gypsum

Morteza Janbaz
University of Wisconsin-Milwaukee

MECHANICAL PROPERTIES AND HIGH-TEMPERATURE PERFORMANCE OF A POLYESTER RESIN MODIFIED USING FGD GYPSUM

by

Morteza Janbaz

A Thesis Submitted in

Partial Fulfillment of the

Requirements for the Degree of

Masters of Science

in Engineering

at

The University of Wisconsin-Milwaukee

December 2013

ABSTRACT

MECHANICAL PROPERTIES AND HIGH-TEMPERATURE PERFORMANCE OF A POLYESTER RESIN MODIFIED USING FGD GYPSUM

by

Morteza Janbaz

The University of Wisconsin-Milwaukee, 2013
Under the Supervision of Professor Habib Tabatabai

High-temperature performance of polyester- based construction materials is an important consideration when fire safety is a concern. These materials are typically used as non-structural components of buildings and other structures. Structural retrofits using fiber-reinforced polymer (FRP) composites are also gaining popularity. However, a major disadvantage of polymer- based materials (including FRP composites) is their flammability and toxic gas generation at high temperatures. The main objective of this research effort was to determine the mechanical properties and high-temperature performance of a polyester resin modified with various amounts of an industrial by-product additive. The additive used was Flu-Gas Desulfurization (FGD) gypsum, which is a byproduct of electricity generation in coal-burning power plants.

Compression and tensile strengths, stiffness, toughness, and impact resistance were measured. Thermo gravimetric analyses (TGA) were also

performed to determinate material loss at a range of temperatures up to1100°C. A limited number of flame combustion tests were also conducted. Experimental results indicate that the tensile strength, stiffness, and energy–absorption capability of polyester resin can be markedly enhanced with the addition of FGD gypsum. TGA results show improved high-temperature performance in polyester resin modified with FGD gypsum and up to 50% of total composite. Under flame exposure, FGD gypsum provides a fire-resistant exterior barrier at the surface of the composite, which serves to protect the interior materials.

TABLE OF CONTENTS

LIST OF FIGURES

LIST OF TABLES

LIST OF ABBREVIATIONS

DSC: Differential Scanning Calorimetry

FGD: Flue Gas Desulfurization

FA F: Class F Fly Ash

FA C: Class C Fly Ash

XRD X-Ray Diffraction

SEM Scanning Electron Microscope

DTG Differential Thermal Gravimetric

TGA Thermo Gravimetric Analysis

DTA Differential Thermal Analysis

MEKP Methyl Ethyl Ketone Peroxide

EPA Environmental Protection Agency

NA Not Available

PPH Parts Per Hundred

PP polypropylene

HDPE High-Density Polyethylene

PMMA Poly (methyl methacrylate)

PVC Poly (vinyl chloride)

P (α-M-S) Poly(α-methyl styrene)

PS Polystyrene

ACKNOWLEDGEMENTS

I would like to thank Professor Habib Tabatabai for his unwavering support through my ups and downs during these last few years that I have been in the United States. My work would not have been possible without his generous insights and contributions. His guidance and support throughout this research and my graduate studies has been considerable.

I would also like to express my appreciation to Professor Konstantin Sobolev for allowing me to use his equipment and providing his kind consideration through the duration of my research work and kindly letting me work for him.

My gratitude goes out to Professor Rani El-Hajjar for allowing me to use his lab facilities, and for providing me with his clear guidance and helping me during the period of time that I was his T.A.

My deepest thanks go out to my dear friend Rahim Reshadi who helped me through some challenging circumstances in the United States. I would like to give a special thanks to all the students who helped me. These students include Scott Muzenski, Mohamadreza Moini, Rebecca Hastings, Sarah Bosch, Nicholas Coley, and all other colleagues. I would like to thank my doctors who kindly helped me during my challenging times.

Finally, I would love to dedicate this work and this last sentence to my parents who raised me. For me, as long as a second is left in my life, they are real love.

1. Introduction and Background

Over the past two decades, there has been increased interest in the use of fiber-reinforced polymer (FRP) composites in civil/structural engineering applications. The primary use of FRP laminated composites has been in the repair and seismic retrofit of structures. FRP laminated composites are wrapped around inadequately-reinforced columns to increase strength and ductility of columns when subjected to earthquake loads. Full-size FRP members have also been used in new construction; however, issues with fire resistance have limited their use to mainly outdoor and some bridge applications. FRP composites offer many advantages over conventional construction materials. They offer corrosion resistance and superior strength to weight ratio. On the other hand, FRP composites are susceptible to significant damage due to high temperatures and flames in fire.

Typical resins used in manufacturing FRP composites (thermosets such as polyester and vinyl ester resins and thermoplastics such as polyethylene and polyurethane) are all extremely flammable and produce significant and toxic smoke. The lack of fire resistance has created significant safety issues and is a major impediment on the way to widespread use of FRP composites and other polyester-based materials in civil/structural applications, especially in indoor applications. Some fire requirements can be satisfied by using fillers in resin, usually alumina trihydrate. On the other hand, some specialized resins containing a halogen such as bromine or additives such as antimony oxide can be used. However, these measures would still not provide complete protection.

Gypsum drywalls are routinely used to achieve sufficient fire ratings in building system, and gypsum is a suitable and code-recognized barrier system for fire resistance. On the other hand, Flue Gas Desulfurization (FGD) Gypsum is a waste byproduct obtained in the process of removing sulfur emissions from coal burning power plant (Figure 1) [15].

These powdered hydrated gypsum byproducts are sometimes used in drywall construction and agricultural applications. Otherwise, they are generally deposited in landfills. This research explores whether FGD gypsum could potentially improve mechanical properties and high-temperature performance of a polyester resin. The effects of varying FGD Gypsum content in a polyester resin were studied.

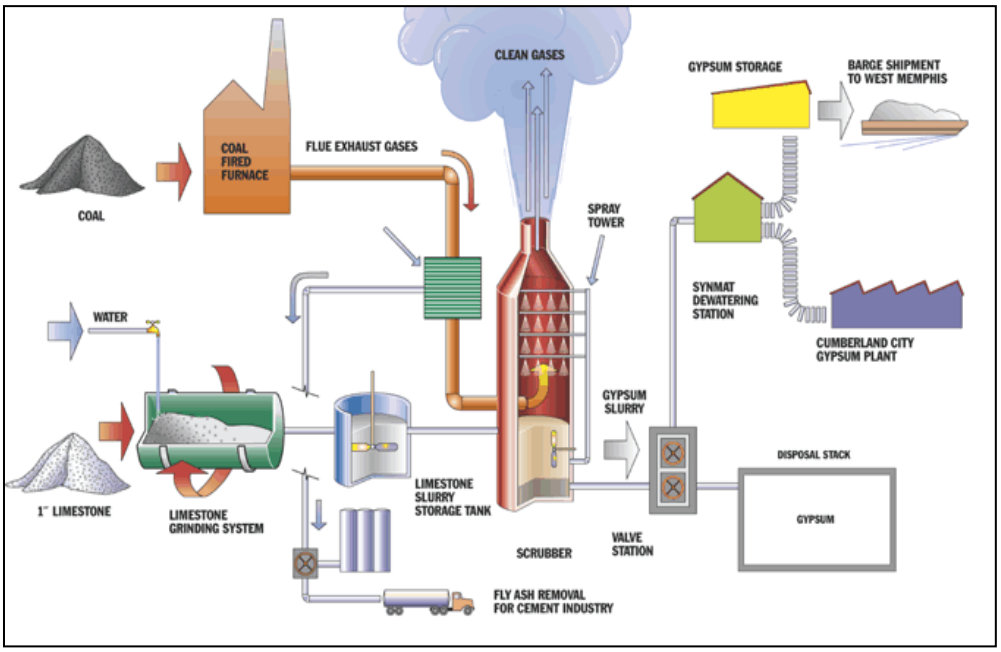

Figure 1: Process for manufacturing synthetic gypsum and fly ash [15].

2. Objective and Scope

The aim of this study was to determine whether FGD Gypsum can be a suitable additive in a polyester resin to improve its mechanical and high-temperature properties. One brand of commercially-available polyester resin ("Captain's Club") was used in this research. FGD gypsum was added at 0, 20, 30, 40, 50, 70, 100, 200, 300, and 400 percent by weight of resin. Compressive and tensile strength tests, stress- strain behavior, pendulum impact tests, TGA, and open flame combustion tests were performed on composites with selected FGD gypsum contents. Scanning Electron Microcopy was used to evaluate size distribution of FGD gypsum as well as fracture surfaces in various resin-FGD gypsum composites.

3. Literature Review

Composite materials are generally made with either a polymeric, metallic, ceramic, or carbon matrix, with polymers being the most widely-used matrices [1]. Polymers can be thermoplastics or thermosets; thermoset polymers do not melt when reheated such as polyesters, epoxies, polyamides, and vinylesters. The physical state of thermoplastic polymers can be softened and changed through heating causing them to melt [1]. Examples of thermoplastics are polypropylene, polysulfone, polyether ether keton, and thermoplastic polyimides [1].

Polyester resins are typically used in FRP composites due to their rapid room-temperature curing, good mechanical properties and relatively low cost. Polyesters are used in a variety of FRP applications such as automotives, boats,

storage tanks, etc. As compared to epoxy resins, polyester resins are more sensitive to elevated temperature [1]. Vinylester composites are ideal in corrosive environments and marine applications due to desirable mechanical and thermal behavior. However, phenolics, which are used in aircraft components, have more heat and fire resistance [1].

Polymers exhibit glass-liquid transitions at their glass transition temperatures, which is the temperature at which the materials change from a glass-like solid into a rubbery material [29].

The combustible nature of polymers creates potential fire hazards and safety issues. Studies have been conducted to evaluate the effects of different additives in fire resistance of resins and FRP composite materials. Such composites are typically evaluated for ignition time of resin, combustion performance, and mechanical performance.

In 2004, a report sponsored by the Federal Aviation Administration (FAA) studied intrinsic relationships between polymer structure, composition, and fire behavior to evaluate fire-safe polymeric materials [27]. The study proposed a combination of three milligram-scale methods to fully characterize the thermal decomposition and flammability of polymers and polymer composites [27]. These methods include pyrolysis-combustion flow calorimetry (PCFC), simultaneous thermal gravimetric analysis (TGA), and pyrolysis gas chromatography/mass spectrometry (GC/MS). The flammability of two groups of intrinsically fire-resistant polymers—polyhydroxyamide (PHA) and its derivatives, and bisphenol C (BPC II) polyarylates were evaluated. Performances were measured using

PCFC, cone calorimeter (ASTM E1354), Ohio State University (OSU) calorimeter, and ASTM E906 test [27]. The report concluded that "PHA and most of its derivatives have extremely low heat release rates and very high char yields upon combustion." BPC II-polyarylate can reportedly be used as an efficient flame-retardant agent in copolymers and blends [27].

The combustion of polymers goes through the following cycle: "(1) heating of the polymer, (2) decomposition, (3) ignition, and (4) combustion," [27]. The polymer decomposes to gaseous products that are combustible if there is an ignition source. Some of the heat generated transfers back to the polymer surface and provides sustainable combustion (Figure 2). Elements such as boron, aluminum, phosphorous, antimony, chlorine and bromine and their compounds are commonly used as base elements for flame retardant additives [27].

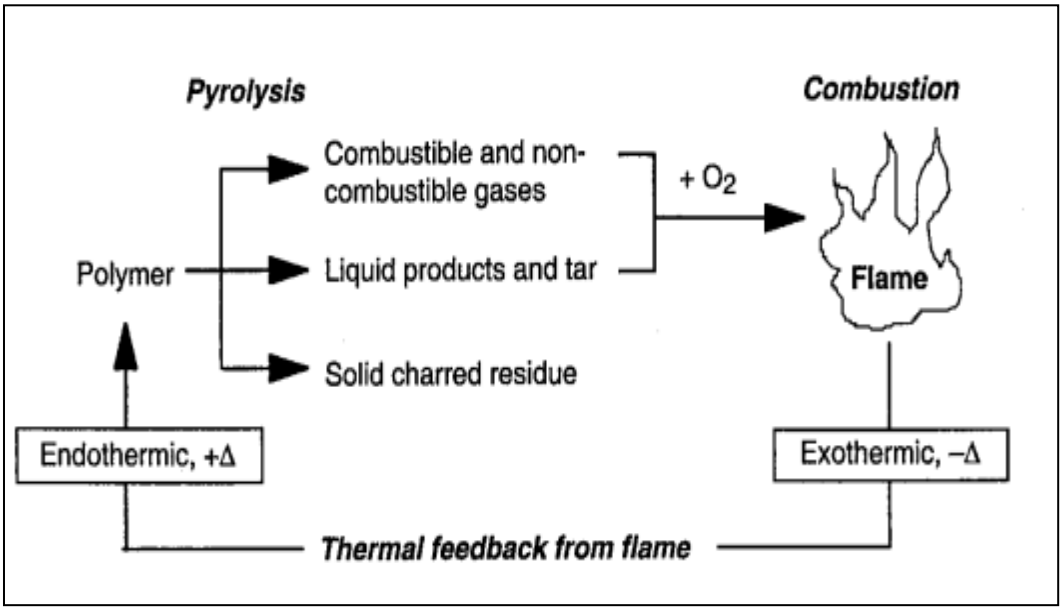

Figure 2: Schematic diagram of polymer combustion [27].

Inhibiting polymer combustion is feasible through two procedures [27]. The most efficient approach would be to produce inherently fire-resistant polymers with high thermal stability. This approach is not easy to accomplish and is expensive [27]. The other procedure includes addition of flame-retardant additives. Two categories of additives react in either chemically-bonded (to polymer) or physically mixed process to provide less flammable polymers [27].

Zhang et al. [27] report on the STA (TGA/DSC) and DTG responses of several aliphatic polymers (Figure 3). It was found that "most aliphatic polymers such as polypropylene (PP), high-density polyethylene (HDPE), and polystyrene (PS) decompose in a single stage with zero char yield, but some polymers such as poly methyl methacrylate (PMMA) and polyvinyl chloride (PVC) decompose in more than one stage." [27].

Yu et al. [2] developed an integrated thermo- mechanical method for predicting the response of FRP to fire using finite element models. Three criteria of load-bearing capacity, integrity and insulation are typically investigated in structural fire resistance studies [2].

Some use intumescent coatings to achieve fire resistance. Wang et al. [3] synthesized a novel phosphorus-containing polymer for amino intumescent fire-resistant coating applications. The experimental results of fire protection tests on plywood board indicated that the fire protection time was significantly extended after application of intumescent coating [3].

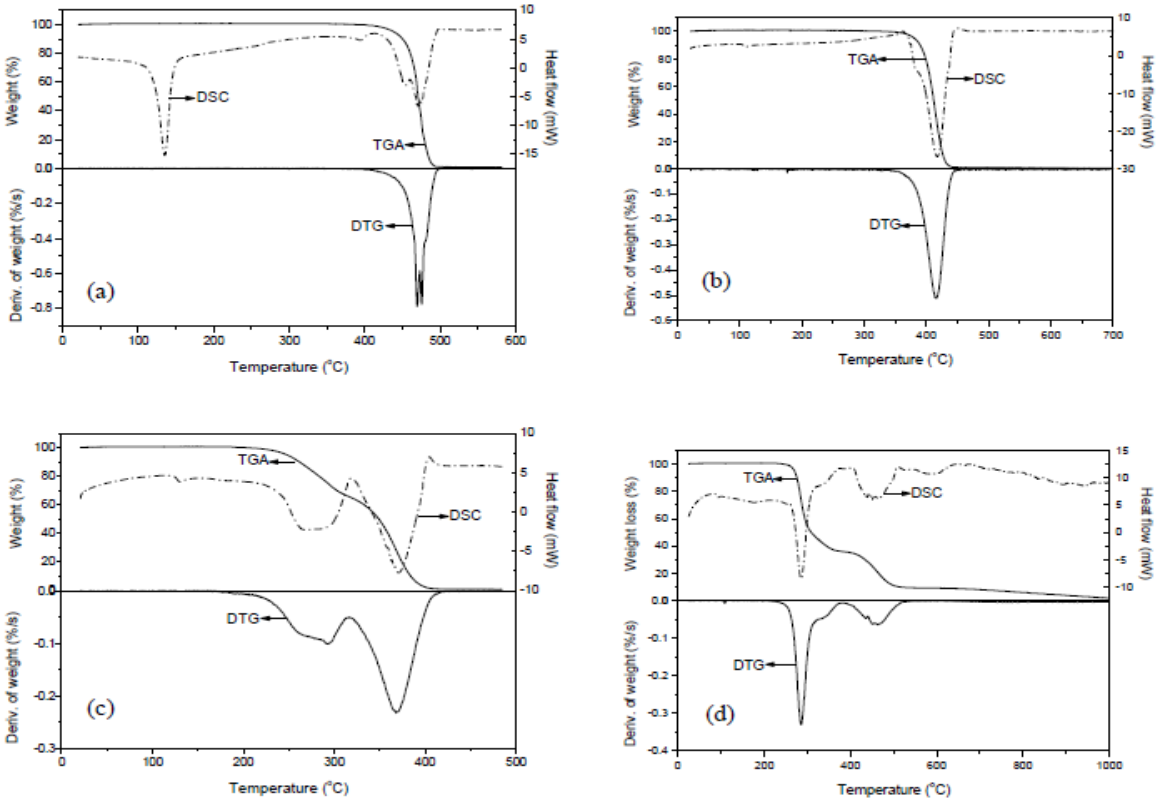

Figure 3: The STA and DTG curves of aliphatic polymers (10°C/min in N2) (a) HDPE, (b) PS, (c) PMMA, and (d) PVC [27].

Ji et al. [4] studied the combustibility of FRP and developed a new fire resistant technology using nanoclay reinforced intumescent coating. The fire retardant coating enhanced the fire resistance and bending strength of RC beams after fire damage [4]. In 2006, Giancaspro studied a thin layer of a fire-resistant paste composed of inorganic geopolymer resin to improve the fire resistance of balsa sandwich panels [5]. The results showed that the intumescing of the geopolymer paste may offer additional fire protection for the sandwich structure [5]. Chiu et al. studied thermal degradation and combustion behavior of unsaturated polyester (UP) resin and a type of Phenolic resin [6]. More recently, researchers evaluated the effect of magnesium hydroxide (MH) on flame

retardation of unsaturated polyester resin [7]. Results show that resin samples containing MH had higher ignition time than samples without MH. Also, total heat release decreased and the flame retardant performance improved with the addition of MH to the unsaturated polyester resin [7].

4. Experimental Approach

4.1. Materials and Test Specimen

The types of polyester resin, hardener and gypsum that were used in this research are described in this section.

Table 1 shows various components of the FGD gypsum – polyester resin composite material that was evaluated in this research.

Table 1: Components of FGD gypsum – polyester resin composite.

Matrix	Polyester Resin ("Captain's Club" Boatyard Resin)
Hardener	Methyl ethyl ketone peroxide (MEKP) (1.56% of matrix weight)
Additive	FGD gypsum supplied by We Energies Corporation (an electric power company)

4.1.1. Polyester Resin and Hardener

Polyester resins are commonly used in the composites industry. These resins are "styrene-based, flammable and catalyzed when combined with Methyl Ethyl Ketone Peroxide" [8]. Methyl ethyl ketone (MEK), also known as

Butanone, is an organic compound with the chemical formulation $CH_3C(O)CH_2CH_3$ [9]. It is a clear substance with the smell of butterscotch and acetone [9]. MEK is soluble in water, and can also be used as a plastic welding agent and for other functions [10]. Table 2 provides the basic properties of the polyester resin used as reported by the supplier [21].

Table 2: Properties of commercial polyester resin "Captain's Club Boatyard Resin" [21].

Color	Red Brown
Viscosity @ 60 rpm	500 to 700 cps
Viscosity @ 6 rpm	1500 to 2800 cps
Thixotropic Index	3 to 4
Specific Gravity	1.1
Mix Ratio	100 to 1 % DDM 9
Gel time (100 gram mass @ 77 F)	30 to 35 min.
Gel to Peak Exo.	9 to 14 min.
Peak Exo-therm	270 to 310 F
Styrene content	< 35 %
Shelf Life	Up to 4 months ***

4.1.2. FGD Gypsum

The creation of natural gypsum starts with very thin crystallization of a mineral called bassanite ($CaSO_4 \cdot 0.5H_2O$) [14]. Homogeneous nucleation of nano crystalline bassanite leads to self-assembly of bassanite into aggregates, and transformation of bassanite into gypsum [14].

Generally, naturally occurring calcium sulfate (natural gypsum) is created in different forms, most common of which are anhydrite ($CaSO_4$) and dihydrate ($CaSO_4\ 2H_2O$) [19]. Flue Gas Desulfurization (FGD) Gypsum is a waste byproduct obtained in the process of removing sulfur emissions from coal-burning power plants. Figure 4 shows the production processes for FGD gypsum

and fly ash as by-product materials [15]. Figure 5 contains an illustration of the process of producing gypsum for commercial uses.

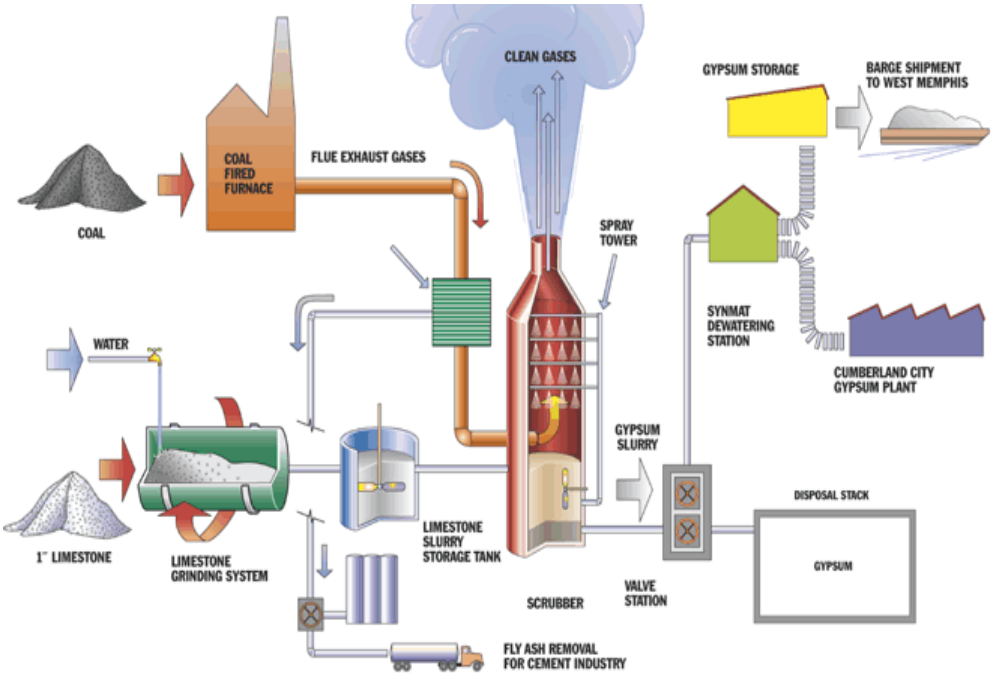

Figure 4: Process for manufacturing synthetic gypsum and fly ash [15].

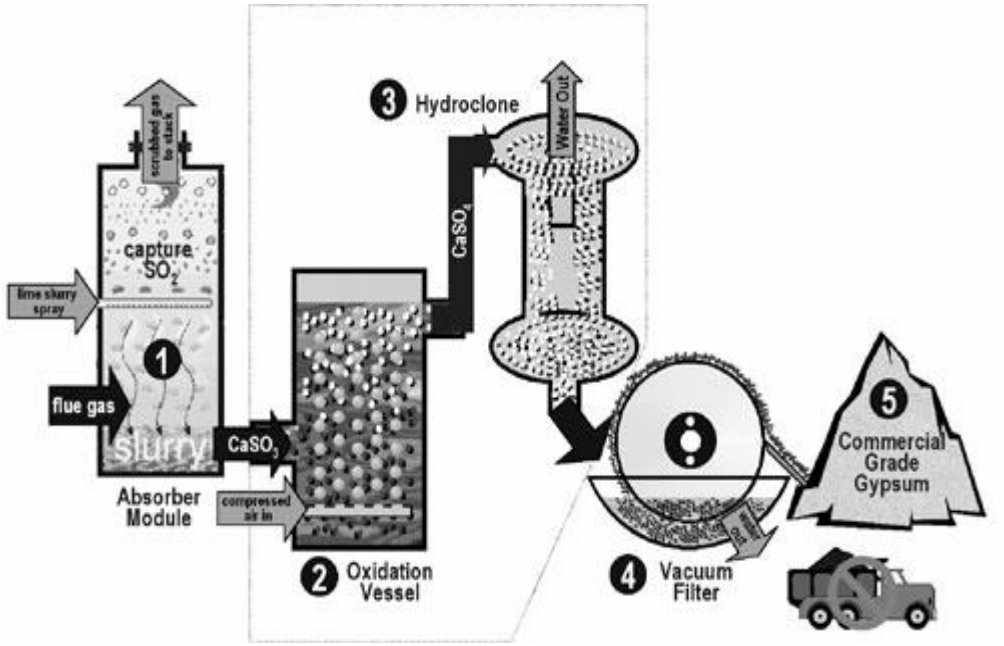

Figure 5: The gypsum production at Zimmer Power Generation Station [18].

FGD gypsum is a very soft powder made up of calcium sulfate dihydrate $CaSO4 \cdot 2H_2O$ [13]. In recent decades, FGD gypsum is sometimes used for the production of drywall or improving farm soils, while the unused materials are deposited in landfills [11]. FGD gypsum can be dissolved in water. One of the most important beneficial uses of FGD gypsum is to mitigate low soil PH problems by spreading it over farmland [12]. Figure 6 shows gypsum's agricultural applications. Figure 7 illustrates the effect of gypsum on shelf life of tomatoes stored at room temperature for two weeks [16].

Figure 6: Gypsum spreading [16].

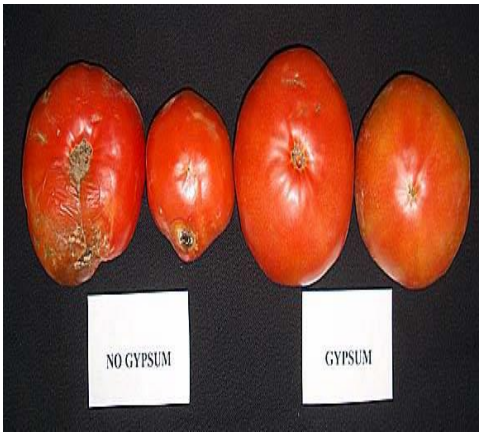

Figure 7: Effect of gypsum on shelf life [16].

Gypsum that has less than 600 parts per million (ppm) of total dissolved solids in the pore water, and a water content of less than 15% by weight is used for drywall manufacture. Gypsum that does not meet this specification is used for agricultural purposes [18].

Table 3 shows water content, particle size, insoluble residue percentage, and price per ton of different types of gypsum [18]. Water content was measured after the samples had been dried overnight at 60° C. The standard deviation of

these reading is given in parentheses. Percentage of Insoluble residue was measured following dissolution for three days at pH < 3 [18].

Table 3: Features of different types of gypsum [18].

Material	**Water content[1] %**	**Particle size**	**Price $/ton**	**Insoluble residue[2] %**
Synthetic gypsum	5.55 (3.04)[3]	120 μm	7.00	0.4 (0.2)
Natural gypsum	0.38 (0.48)	NA	12.75	12.9 (8.1)
Cast gypsum[4]	0.15 (0.21)	NA	NA	0.2
Drywall gypsum	10.1 (12.8)	< 0.5 inch	11.00	2.2 (0.3)
1 Dried overnight at 60 degrees Celsius.				
2 Following dissolution for three days at pH < 3.				
3 Standard deviation included in parentheses.				
4 Material is not yet available for sale for agricultural application.				
NA = not available				

Figure 8 displays a Scanning Electron Microscope (SEM) image of FGD gypsum with magnification of 200x. This FGD gypsum was produced at a We Energies power plant in Wisconsin. Figure 9 shows the FGD gypsum particle size distribution, as reported by We Energies Corporation [17].

Table 4 presents the typical characteristics of We Energies' FGD gypsum [17].

Figure 8: FGD gypsum with magnification of 200x.

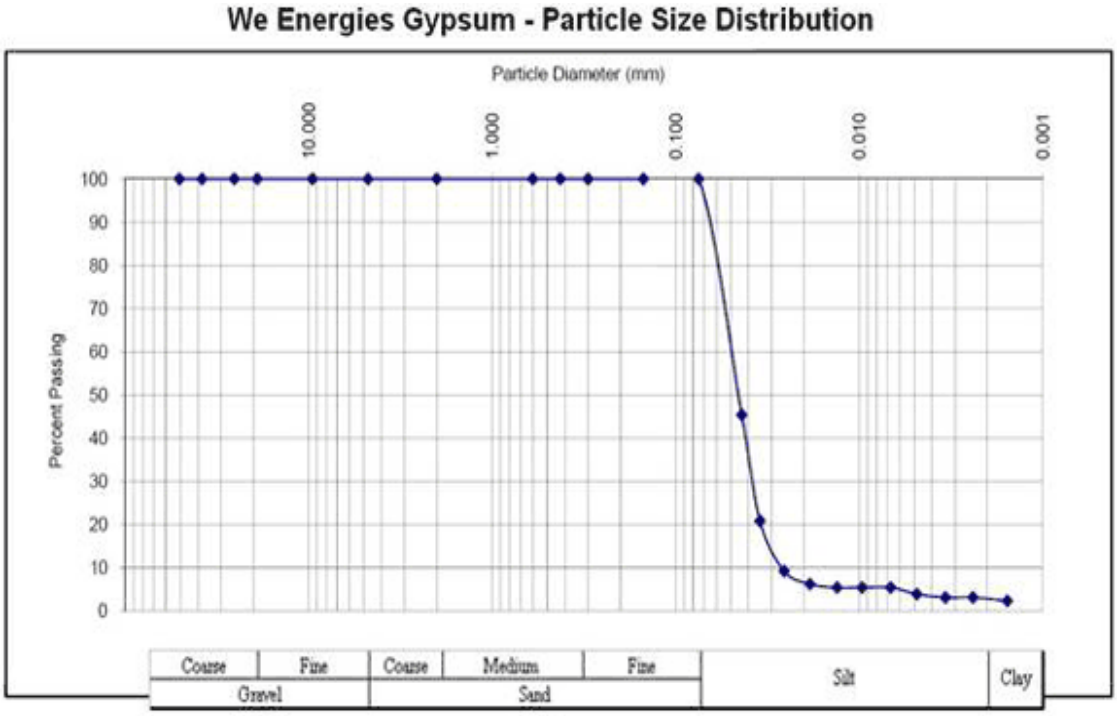

Figure 9: We Energies Gypsum-Particle Size Distribution[17]

Table 4: Typical characteristics We Energy's FGD gypsum (dry basis)[17].

Purity ($CaSO_4 \cdot 2H_2O$)	> 95%
Calcium content	> 20%
Sulfur content	> 16%
Particle Size - % passing 200 mesh sieve	> 95%
Angle of Repose	49°

4.1.3. Preparation of Polyester- Resin FGD Gypsum Composites

In this work, the amount of FGD gypsum added to polyester is typically described as parts per hundred (PPH) parts of polyester resin. For example, a reference to R70 mix indicates that the proportion of FGD gypsum to polyester resin (by weight) was 70 to 100. Therefore the percentage of FGD gypsum in R70 polyester–gypsum composite is 41.2% (or 70 divided by 70 +100) (Table 5).

The FGD gypsum was first air dried at room temperature, and was subsequently sieved using a #100 sieve before the mixing process. Polyester resin and hardener were first mixed together and stirred for about one minute by hand mixing in a sealed plastic bag. Then, the FGD gypsum was added in and hand mixed until a uniform distribution was achieved (Figure 10). Different proportions of FGD gypsum were mixed with the polyester resin, with gypsum content of up to 83% (83% gypsum, 17% resin) as shown in Table 5.

Table 5: Mixtures of polyester resin, hardener and different proportions of FGD gypsum used.

Specimen	PPH Gypsum:100 Resin	%Gypsum (of total wt)	%Resin (of total wt)
R0	0	0	100
R10	10	9.1	90.9
R20	20	16.67	83.33
R30	30	23.1	76.93
R40	40	28.57	41.43
R50	50	33.33	66.67
R70	70	41.2	58.8
R100	100	50	50
R200	200	66.7	33.3
R400	400	80	20
R500	500	83.33	16.67

Figure 10: Simple hand mixing of gypsum and resin and hardener.

4.2.1. Compression tests

Cubic samples (2 in or 50.8 mm) were prepared for compressive strength testing of the gypsum-polyester composite. Each 2-in cube mold was first covered by Teflon sheet for ease of de-molding. Selected FGD- modified resin proportions were placed into 2-in cube molds in two layers, with each layer being tamped using a metal tamper. The cube molds were covered with glass plates and placed at room temperature (70-80° F). The specimens were then demolded after 24 hours.

Compressive tests on 50.8 x 50.8 x 50.8 mm cubes were performed in accordance with ASTM C109 (Standard Test Method for Compressive Strength of Hydraulic Cement Mortars). These specimens were tested using an ADR-Auto ELE compression machine (Figure 11) and loaded at a rate of 0.9 KN/sec. The maximum load and maximum compressive stress achieved were recorded.

Figure 11: ADR-Auto ELE Compression Machine [22].

4.3.1 Tensile Tests

A set of dog-bone-shaped molds were made for tensile test specimens (Figure 12). The molds were made from one hand-cut Teflon sheet connected together with another Teflon sheet using screws. Teflon was used to allow de-molding as resin will adhere to other mold materials. The dog-bone molds were filled with the FGD-modified resin. Figure 12 shows the dimensions of dog-bone specimens. Actual dimensions of the dog-bone specimens were measured after demolding. In order to securely fasten the dog-bone into the test machine grips, a scratch polisher machine was used to increase the surface roughness at the grip area to reduce potential for slip.

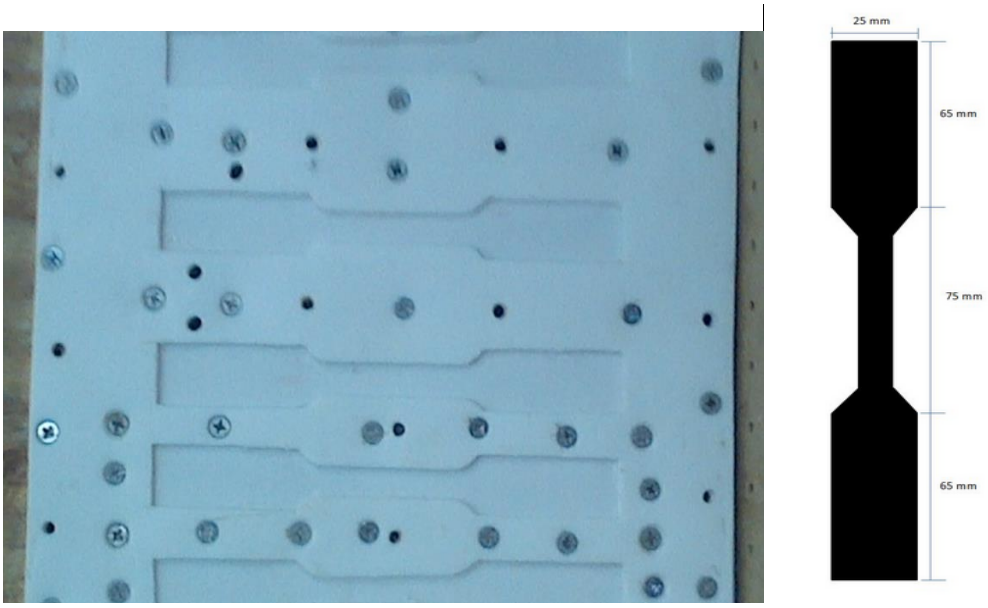

Figure 12: Dog bone Teflon mold used to obtain uniformly shaped and easily removable samples.

Tensile strength and elongation of the cast FGD-modified resin were obtained based on ASTM D638 (Standard Test Method for Tensile Properties of Plastics). These tests were performed using an Instron tensile testing machine (Figure 13 and Figure 14). The load was monitored using the test machine's load cell, and strain was measured using an extensometer (Model 2630-115) with a gage length of 50mm (2 in).

Figure 13: Instron Testing Machine

Figure 14: Sample testing on Instron Machine

4.4.1 Pendulum Impact Tests

Impact resistance was tested using a Tinius Olsen Pendulum Impact Machine (Model 104) as per ASTM D256 (Standard Test Methods for Determining the Izod Pendulum Impact Resistance of Plastics). Pendulum Impact Machines are designed to determine the energy absorbed by the plastic upon impact by a pendulum hammer. The Tinius Olsen pendulum impact machine consists of a base in which the sample can be mounted (Figure 15). A rigid frame surrounds the pendulum, which can be locked and secured for safety reasons. The specimen rests against two supports on either side of the notch test specimen (Figure 16).

Figure 15: Model 104 Pendulum Impact Display

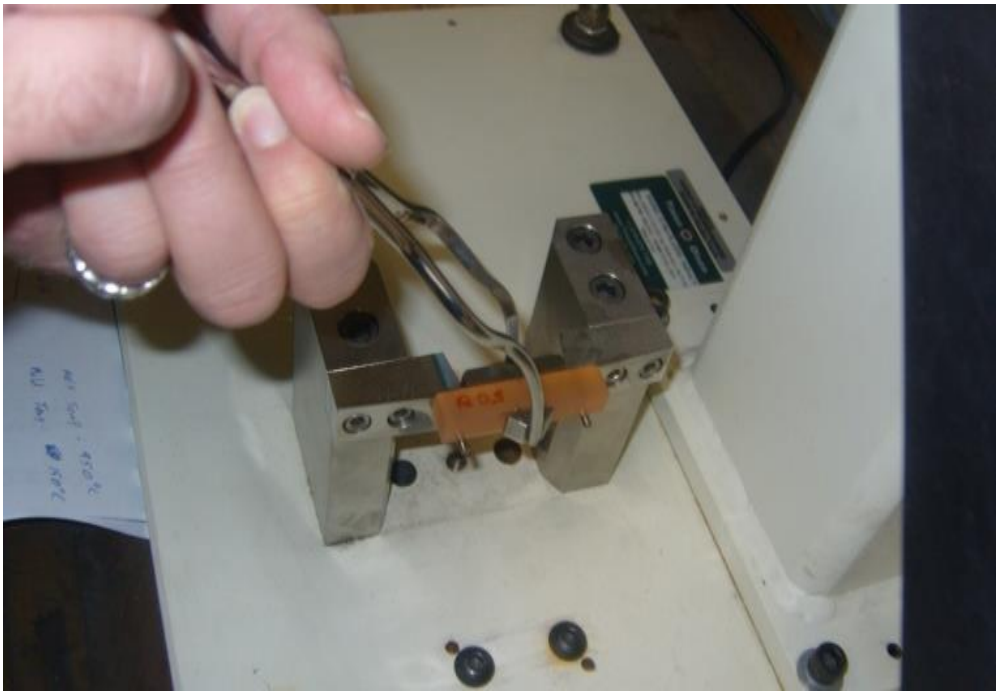

Figure 16: Two supports on either side of a test notch

Pendulum impact testing is a high strain-rate test that measures the amount of energy absorbed by a material during fracture. This energy is equivalent to the difference in gravitational potential energy of the mass located at the end of a pendulum before and after striking a notched rectangular sample. In addition to recording the total impact energy, the machine also records the impact energy per unit area (STRE1) and per unit notch width (STRE2).

Specimens are specially designed with a milled notch to ensure a brittle fracture through a stress concentration. Specimens consisted of 55 x 10 x 10mm blocks. The V notch has 0.25 millimeters radius with a 45-degrees angle, is 2mm deep and runs parallel to the base (Figure 17) [23].

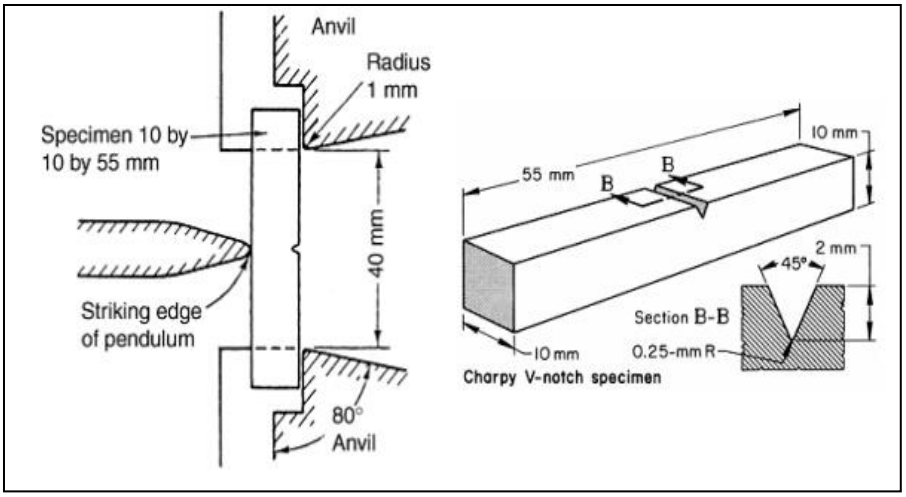

Figure 17: Standard pendulum impact test setup and test specimen [23].

4.4.2 Preparation of V Notch Specimens

Rectangular molds were lined with Teflon and filled with FGD gypsum-polyester composite in two lifts, with each lift being compacted using a metal tamper. The molds were placed at room temperature (70-80°F). The specimens were then removed from the molds approximately 24 hours after casting. After demolding and milling the samples (Figure 18), a notch was milled on each specimen (Figure 19) and the impact tests were performed.

Figure 18: Milling samples before creating the notch

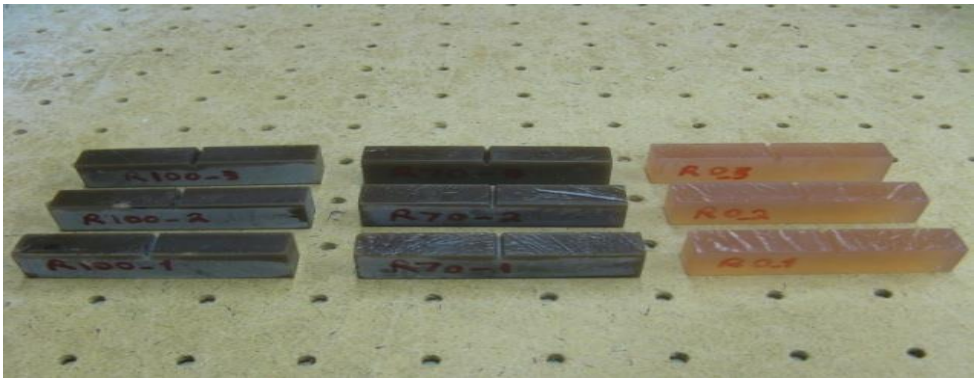

Figure 19: Samples after milling process and applying the notch

The initial potential energy measured was 2.1702 Joules. This was determined by calibrating a zero potential energy in a "free hanging" position, and conducting a windage and friction calibration with a "free swing" of the pendulum without a specimen. The impact energy is the potential energy that is absorbed by the specimen as measured by the difference between the initial potential energy and the final potential energy of the pendulum after pendulum impact; the potential energy difference is recorded automatically by the test machine.

4.5.1. Open Flame Tests

To conduct a preliminary assessment of relative combustibility, cube specimens made using the procedure described earlier were also subjected to open flame from a torch. Cubic samples were placed on a metal tray and subjected to direct flames from a torch with temperature of up to 1100°C for 20 minutes (Figure 20).

Figure 20: Cubic specimen subjected to direct flame.

4.6.1. TGA Tests

The Thermogravimetric Analysis (TGA) is a technique in which the characteristics of a mass is examined as a function of temperature and/or time as the sample specimen is tested under an increasing temperature, in a controlled atmosphere. In most TGA tests, the test material's reduction in mass with increasing temperatures is monitored and recorded. This test is performed in a controlled furnace in which the sample rests on a very precise scale. The atmosphere within the furnace is normally controlled using either an inert or a reactive gas in order to limit outside variables. The machine records all the weight data on a chart, which displays the TGA results measured in weight (mass) percent as a function of temperature. From this curve one can observe weight trends with temperature [24]. In this test, a TA instrument (SDT 2969) was used to record data (Figure 21).

The TGA results can be used to determine the derivative thermogravimetry (DTG) by taking a derivative of the mass versus temperature result. The rate of mass change (DTG) is useful in identifying temperatures at which major mass losses occur. As shown in Figure 3, the rapid loss of mass and decomposition for most common polymers occurs at temperatures ranging from 250 to 500°C. Additives that can prevent and delay decomposition (until higher temperatures) will improve fire resistance.

Figure 21: TGA Machine (Model TA Instrument SDT 2960)

4.7.1. SEM

The Scanning Electron Microscope (SEM) utilizes electron beams to obtain high magnification images of surfaces. The magnified images were used to assess the micro-structure of the fracture surface of the dog-bone tensile specimens in this study. A "Top Con" ABT-32 SEM machine was used to produce high quality resolution images with magnifications of 50X to 5,000X (Figure 22). Selected polyester – gypsum composite fracture surfaces (R0, R100, R300) were examined using SEM.

Figure 22: Top Con ABT-32 SEM Machine

5. Results

5.1 Compressive Strength

Table 6 shows measured compressive strength at different percentages of FGD gypsum. One cube was tested at each FGD content level. Figure 23 shows variations in compressive strength of polyester-resin FGD gypsum composite as a function of the percentage of gypsum content. There is an overall reduction in compressive strength as FGD content is increased. However, because of the limited number of samples tested and the limited number of FGD content variations, the relationship cannot be well defined at this time. In all FGD-gypsum resin tests, the color of the material changed to a beige color just before failure (brown to beige) (Figure 24 and Figure 25).

Table 6: Variation of compressive strength of polyester-resin FGD gypsum composites.

Specimen	% FGD Gypsum	Strength (MPa)	Strength (PSI)
R20	16.7	115.8	16,795
R50	33.3	82.9	12,024
R200	66.7	63.0	9,137
R500	83.3	11.3	1,639

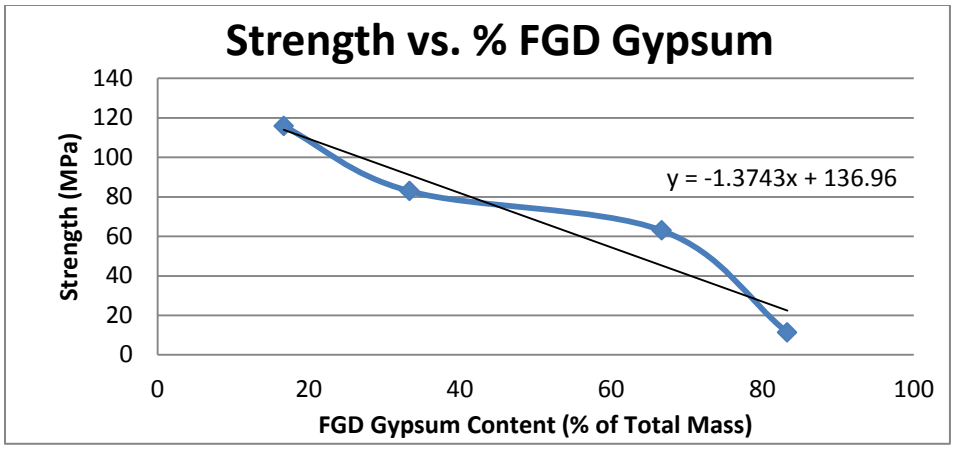

Figure 23: Variation of compressive strength of polyester-resin FGD gypsum composites as a function of FGD gypsum content.

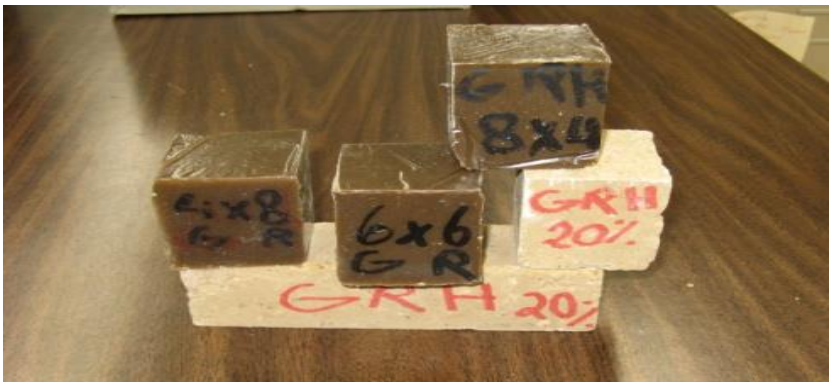

Figure 24: Various compressive test specimens of polyester-resin FGD gypsum.

Figure 25: Color changes in sample at failure.

5.2 Open Flame Tests

The combustion tests (Figure 26 through Figure 30) showed that the bulk of the resin mixed in with FGD gypsum did not ignite even after 20 minutes of exposure to fire. Although the specimens did sustain charring on the surface during the flame tests, the residual gypsum on the surface worked as a protective wall to save the rest of the composite (Figure 28). Figure 29 and Figure 30 show a saw-cut cross section of R70 and R100 specimens after exposure to the open flame test. The protective zone in the R70 specimen is clearly observable (approximately 5mm thick). The R100 specimen had a thinner protective layer (approximately 1mm). As expected, resins with higher FGD gypsum performed much better in combustion tests (Figure 30).

Figure 26: Polyester Resin- FGD gypsum composite specimen subjected to open flame.

Figure 27: FGD- modified resin sample subjected to open flame from a torch.

Figure 28: The charred surface of the R70 cube specimen.

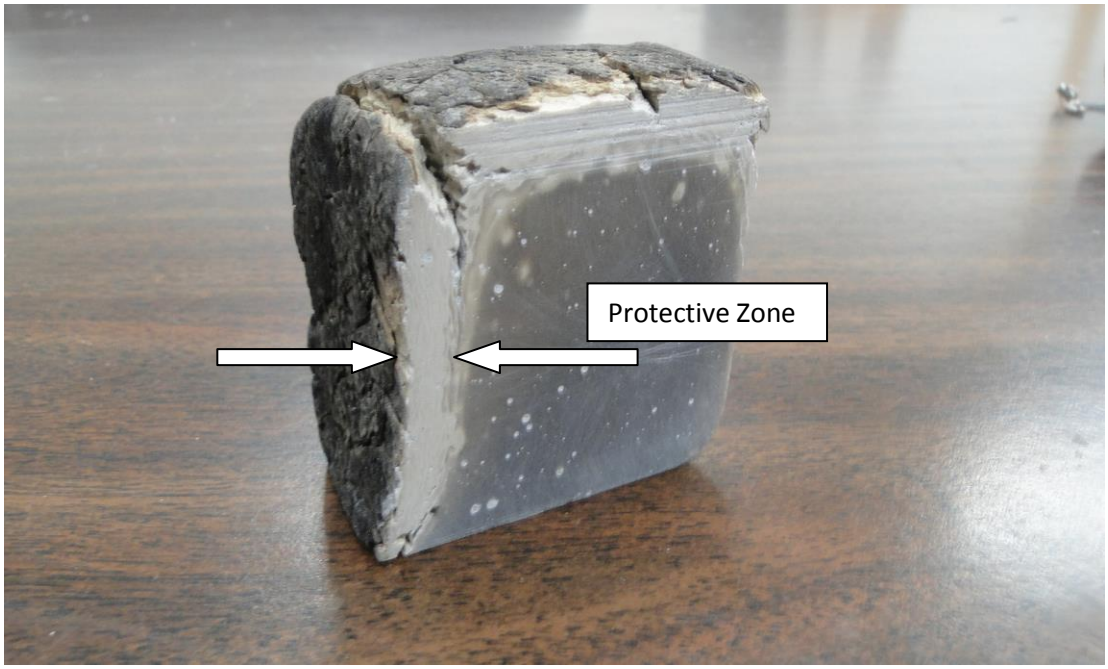

Figure 29: A saw-cut cross section of R70 specimen subjected to flame test.

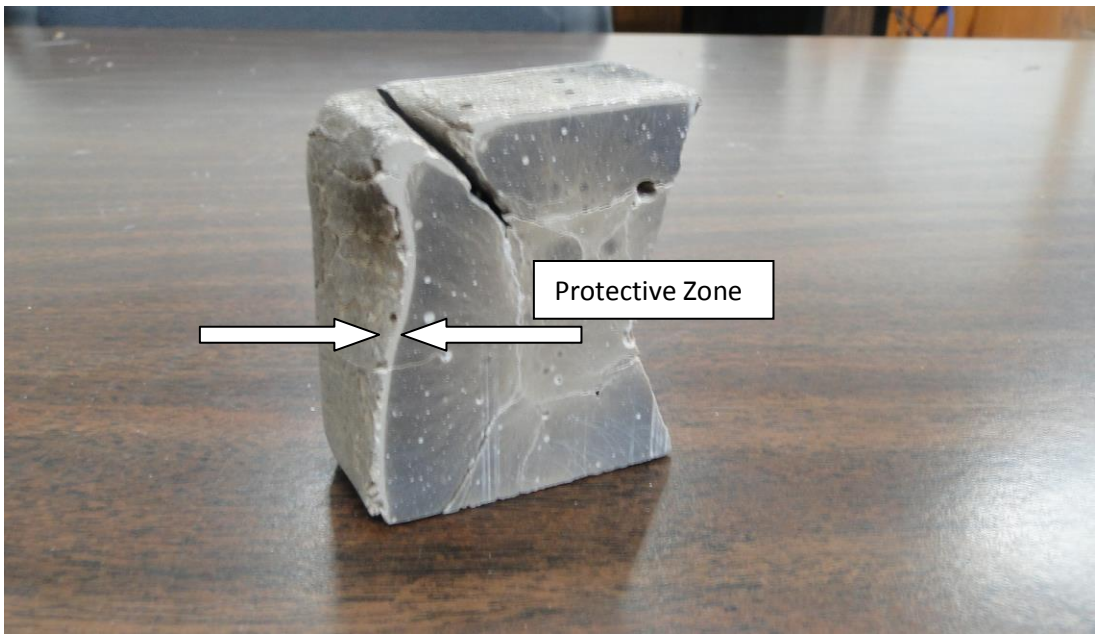

Figure 30: A saw-cut cross section of R100 specimen subjected to flame test.

5.3 Tensile Strength

Stresses and strains were determined during tensile testing of samples with different percentages of FGD gypsum. The stress-strain response was used to determine maximum stress (strength), strain corresponding to maximum stress, and energy per unit volume (area under the stress-strain curve) as well as three different moduli of elasticity. The "initial modulus" was determined based on the initial slope of the stress-strain curve. The "secant modulus" was the slope of a line connecting the origin to the highest stress point in the diagram. The "peak modulus" was the slope of a tangent to the stress-strain diagram at the peak stress.

As shown in Table 7, the tensile strength was increased by adding FGD gypsum in the polyester resin up to R100; however, the maximum strength decreased between R200 and R400. The tensile strength significantly reduced in the R400 specimen. Table 7 also shows strain values at maximum stress. The maximum strain slightly increased, but subsequently decreased with increase in FGD gypsum content.

Table 8 shows an overall increase in energy absorption capability (area under the stress-strain diagram up to peak stress) up to R100. The energy absorbed by samples decreased at FGD contents higher than to R300.

Table 7: Variations in stress and strain in resin-FGD gypsum composites.

Specimen Number	pph (G/R)* 100	Average Area	FGD Gypsum Content (G)	Polyester Resin content (R)	Peak Load	Average Peak Load	Maximum Stress	Average of Maximum stress	Strain at Max Stress	Average Strain at Maximum Stress
		(in2)	(grams)	(grams)	lbf	lbf	Psi	psi	%	%
R0-1	0	0.070	0	125	117.5	117	1686	1616	0.463	0.440
R0-2	0	0.071	0	125	125.8		1772		0.531	
R0-3	0	0.075	0	125	103.7		1390		0.343	
R30-1	30	0.066	37.5	125	176.1	138	2671	2002	0.550	0.460
R30-2	30	0.070	37.5	125	149.2		2055		0.443	
R30-3	30	0.070	37.5	125	117.45		1668		0.463	
R30-4	30	0.067	37.5	125	108.7		1613		0.382	
R50-1	50	0.073	62.5	125	127.3	140	1733	1912	0.287	0.360
R50-2	50	0.079	62.5	125	166.3		2103		0.46	
R50-3	50	0.066	62.5	125	125.2		1901		0.344	
R70-1	70	0.074	87.5	125	192.9	191	2604	2536	0.383	0.375
R70-2	70	0.076	87.5	125	185.7		2455		0.366	
R70-3	70	0.076	87.5	125	195.1		2550		0.377	
R100-1	100	0.066	125	125	184.9	198	2809	2713	0.436	0.390
R100-2	100	0.080	125	125	207.0		2585		0.357	
R100-3	100	0.075	125	125	203.3		2745		0.379	
R200-1	200	0.073	250	125	230.4	185	3156	2572	0.282	0.21
R200-2	200	0.066	250	125	145.2		2190		0.191	
R200-3	200	0.076	250	125	180.2		2370		0.171	
R300-1	300	0.066	375	125	110.4	102	1690	1467	0.199	0.154
R300-2	300	0.070	375	125	116.4		1672		0.178	
R300-3	300	0.076	375	125	79.2		1038		0.086	
R400-1	400	0.073	500	125	24.4	19	322	252	0.062	0.060
400-2	400	0.073	500	125	6.7		92		0.04	
R400-3	400	0.075	500	125	25.1		338		0.079	

Figure 31 shows the variation of tensile strength with PPH. A polynomial trend line shows that the maximum tensile strength occurs at a PPH of approximately 100.

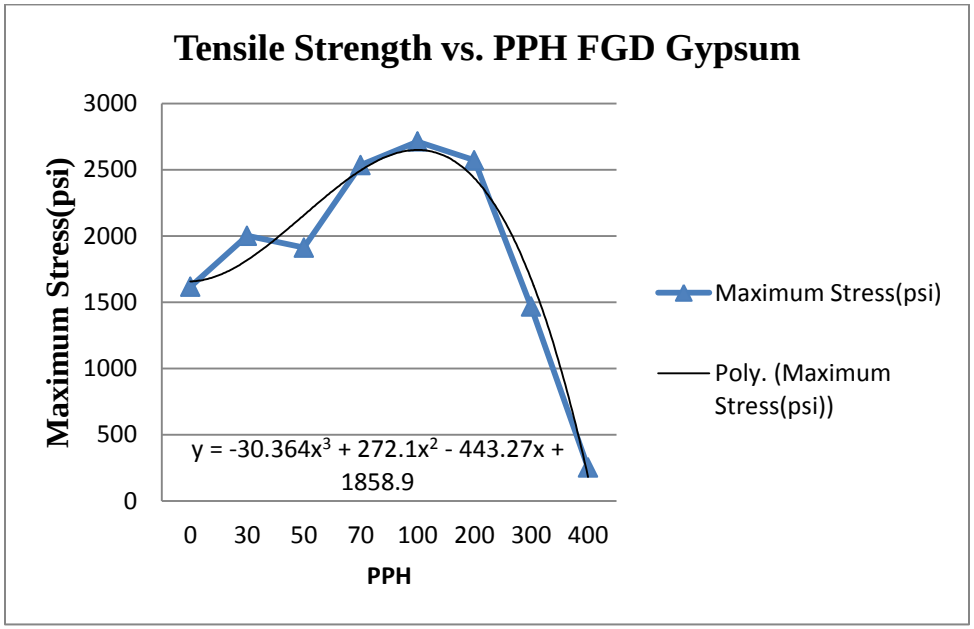

Figure 31: Maximum stress values vs. PPH FGD gypsum.

In general, the moduli of elasticity also increase with increasing FGD gypsum content all the way up to a PPH of 200, after which the moduli decrease (Table 8 and Figure 32). Figure 33 shows variations of the initial modulus of elasticity with PPH, as well as a polynomial trendline. Figure 34 shows the average energy/volume values across the different PPH levels.

Figure 35 shows the stress-strain analyses for the R0 specimens, which did not contain any FGD gypsum. Figure 36 through Figure 42 displays the stress-strain analyses for all other specimens with varying FGD gypsum contents.

Table 8: Mechanical properties during tensile testing.

File Name	E Peak (psi)	Average of E peak (psi)	E Initial (psi)	Average of E Initial (psi)	E Secant (psi)	Average of E Secant (psi)	Energy/Volume (psi)	Average of Energy/Volume (psi)
R0-1	3479	3629	3631	4059	3644	3667	393	371
R0-2	3416		4066		3334		477	
R0-3	3991		4480		4053		243	
R30-1	3928	4153	6197	4588	4854	4331	784	481
R30-2	4177		4912		4635		472	
R30-3	3443		3593		3606		388	
R30-4	5065		3650		4227		278	
R50-1	5450	4757	7392	5867	5997	5351	249	346
R50-2	3974		4440		4540		479	
R50-3	4849		5769		5515		311	
R70-1	4696	5199	9036	9016	6802	6745	548	499
R70-2	5083		11727		6670		501	
R70-3	5818		6285		6764		449	
R100-1	3689	4416	12872	9204	6447	6979	701	606
R100-2	5319		8670		7243		501	
R100-3	4240		6069		7246		618	
R200-1	9540	10155	8375	11743	11193	12113	422	283
R200-2	10804		15931		13725		215	
R200-3	10123		10940		11421		212	
R300-1	8222	9002	10940	10734	8429	8910	166	156
R300-2	9781		10527		9390		146	
R300-3*	23643*		8872*		12033*		37*	
R400-1	2042	2832	8404	5471	5147	4290	14	8.9
R400-2	1130		2523		2252		2.2	
R400-3	5323		5487		5471		10.5	

*Out- of- range. Not included in average value

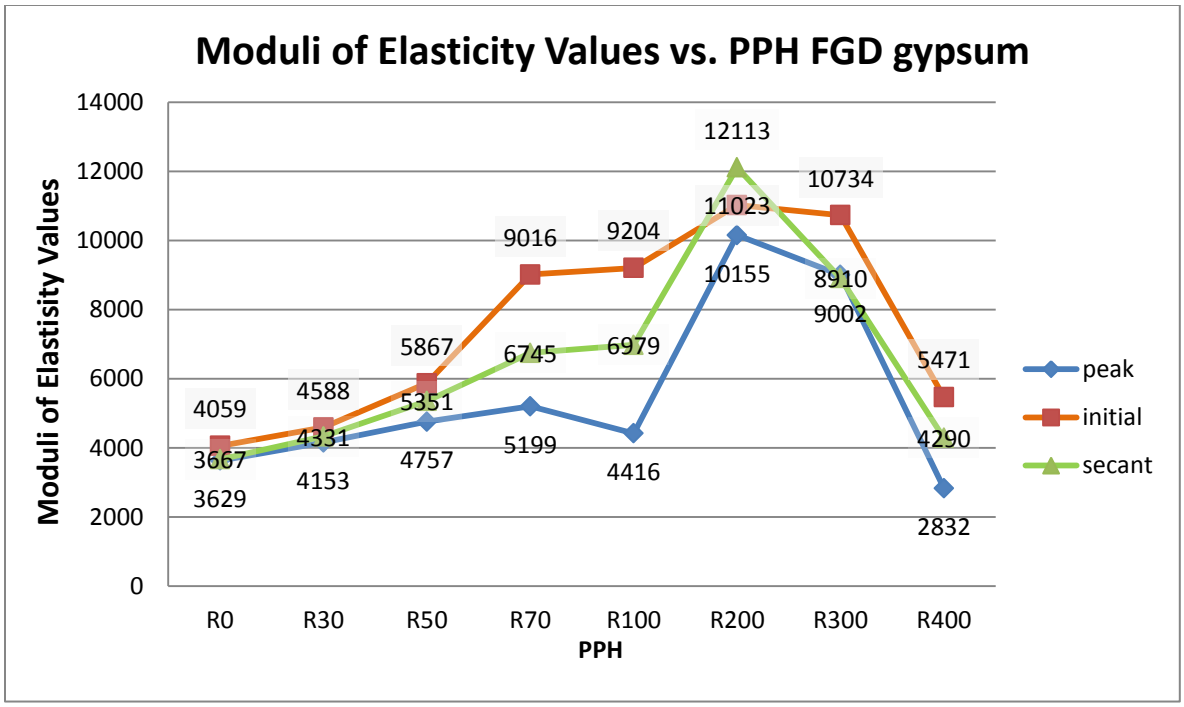

Figure 32: Initial, secant, and peak moduli of elasticity for different proportions of FGD gypsum.

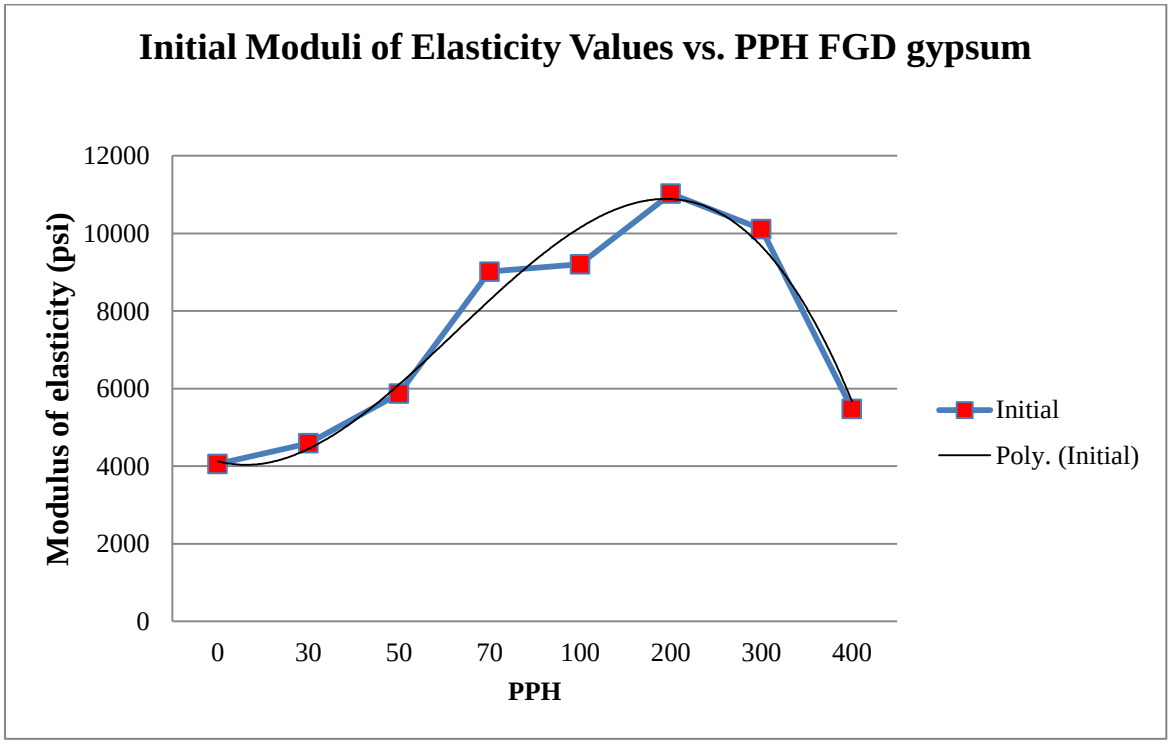

Figure 33: Initial moduli of elasticity for different proportions of FGD gypsum.

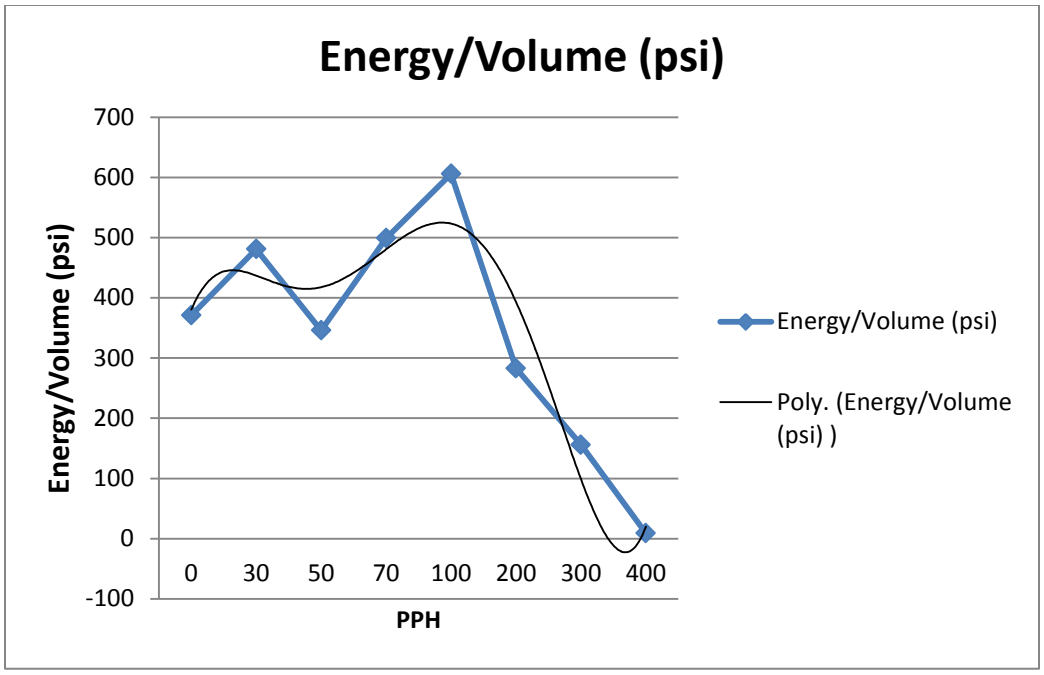

Figure 34: Energy/volume vs PPH FGD gypsum .

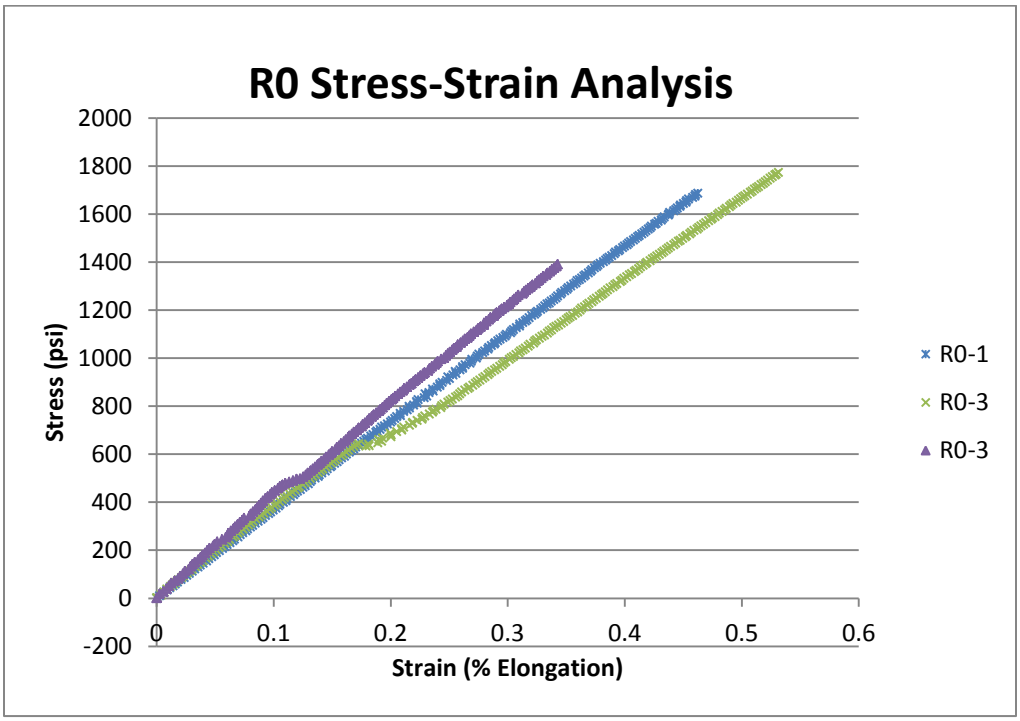

Figure 35: Stress strain diagram for R0 specimens.

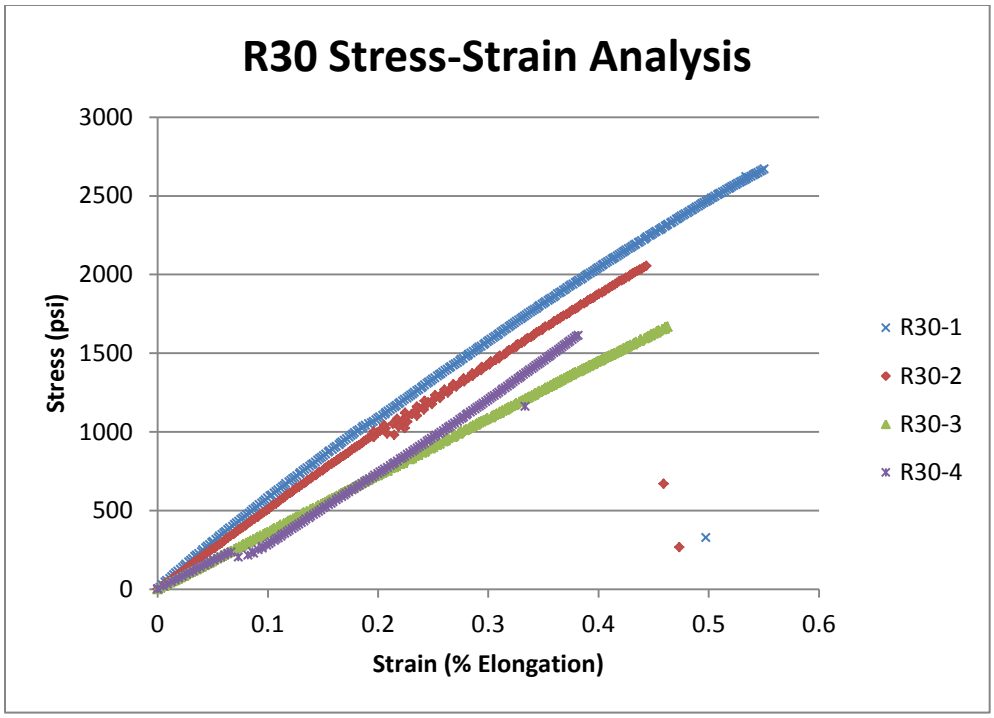

Figure 36: Stress strain diagram for R30 specimens

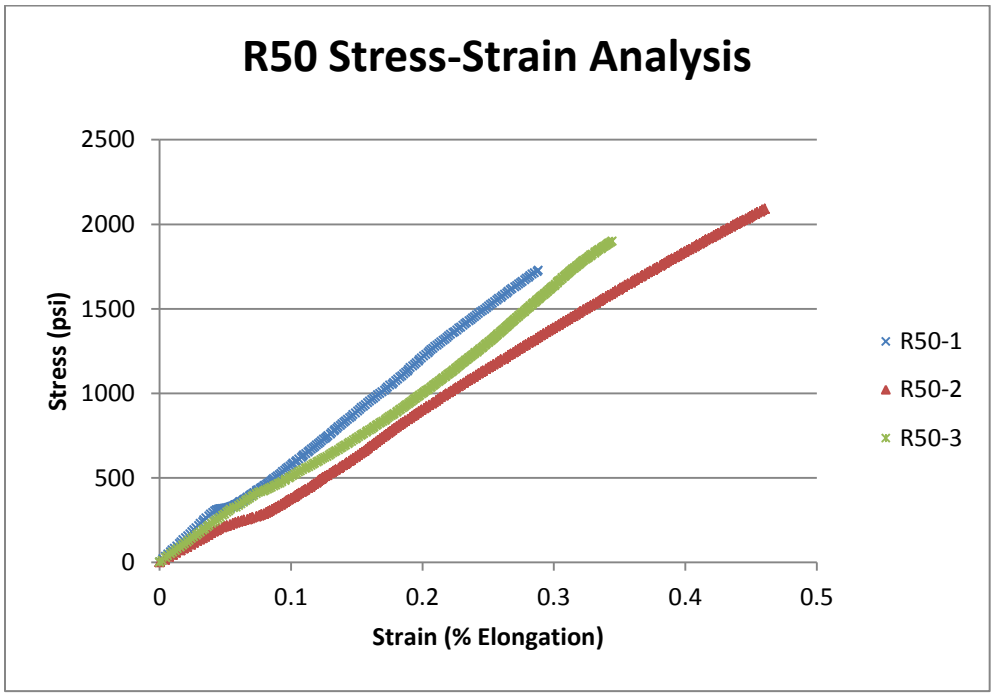

Figure 37: Stress strain diagram for R50 specimens

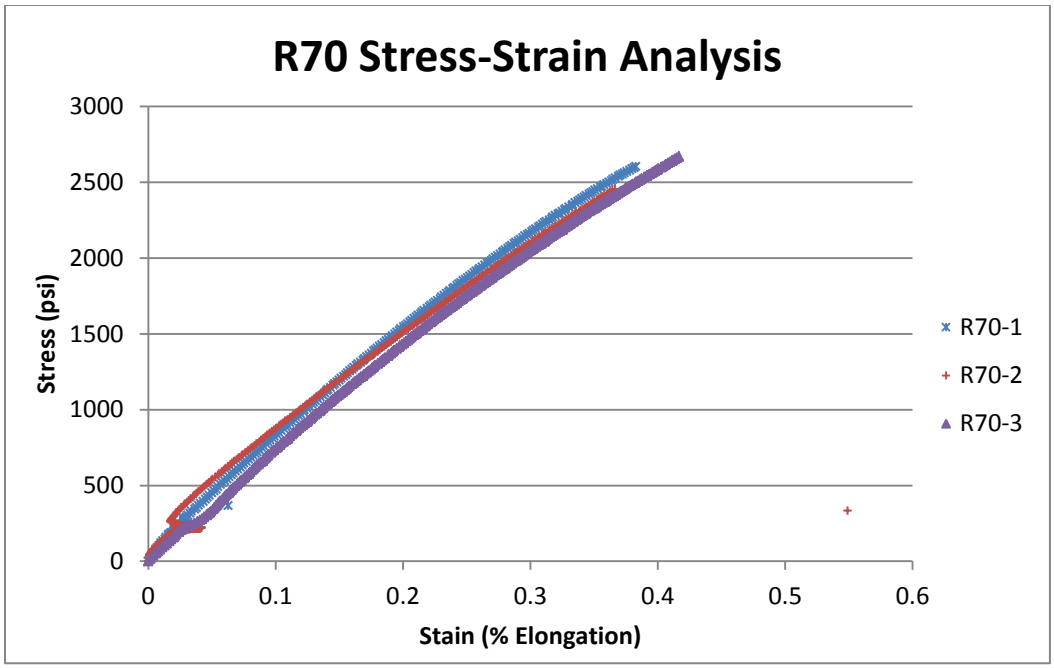

Figure 38: Stress strain diagram for R70 specimens

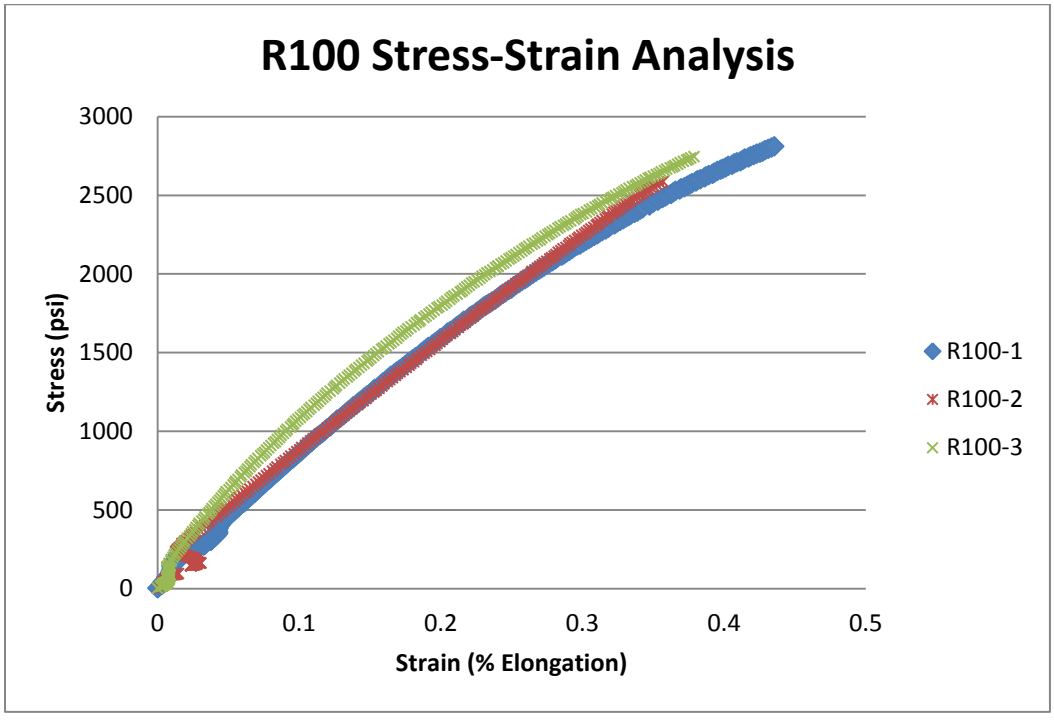

Figure 39: Stress strain diagram for R100 specimens.

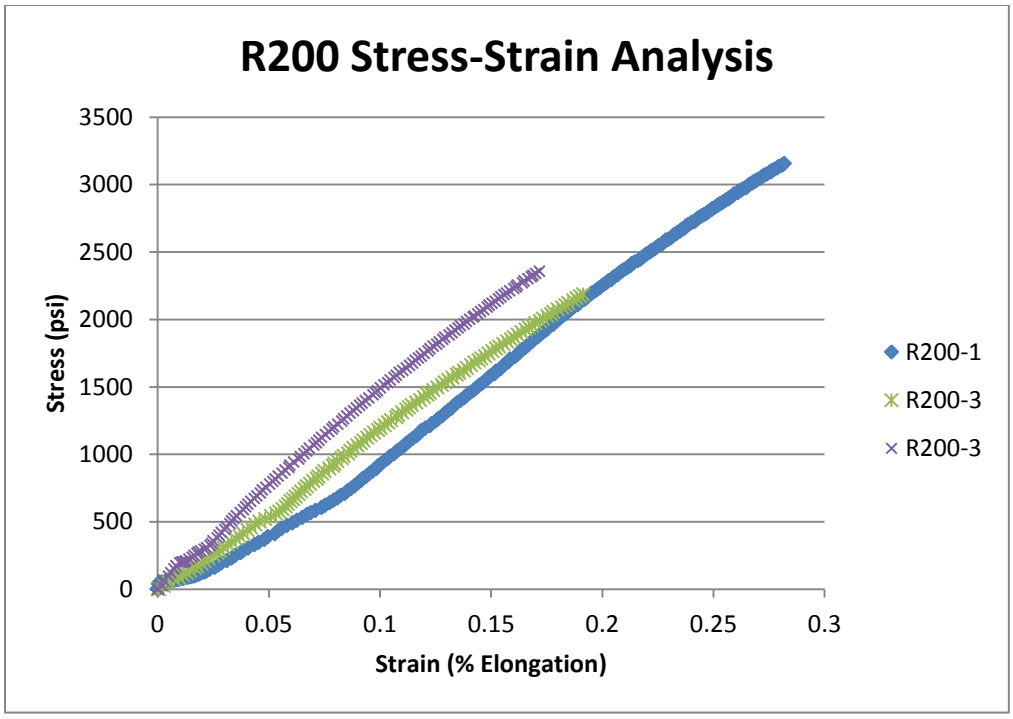

Figure 40: Stress strain diagram for R200 specimens.

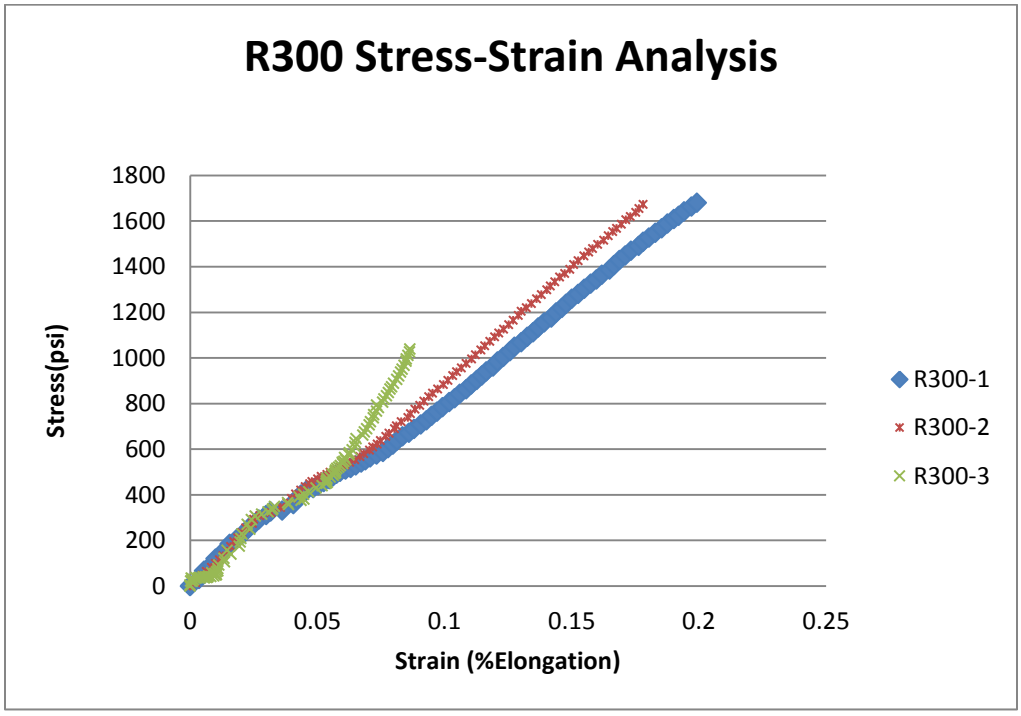

Figure 41: Stress strain diagram for R300 specimens.

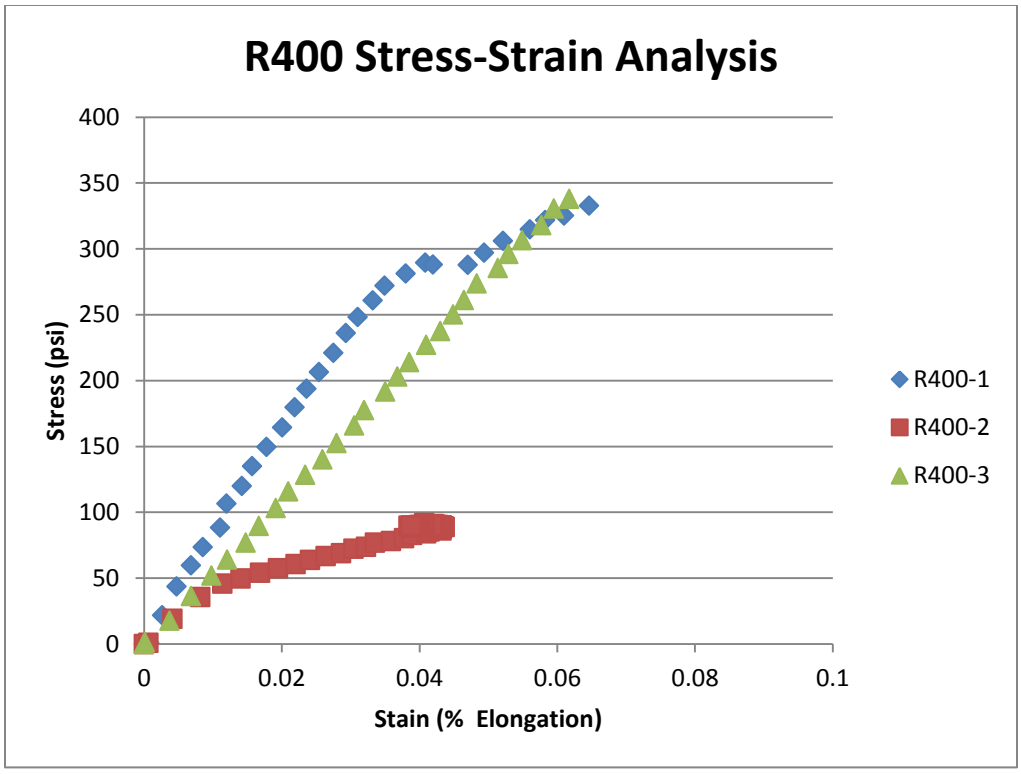

Figure 42: Stress strain diagram for R400 specimens.

Figure 43 shows comparisons of the stress-strain relationships for R0 through R400. Figure 44 plots the average maximum stresses for each PPH versus the average strain corresponding to the maximum stress. R100 and R200 had the highest average peak stress. R0 and R400 had lower strengths and moduli of elasticity than the R70 and R100 samples. Overall the tests demonstrated an increase in tensile strength up to R100 and an increase in modulus of elasticity up to R200.

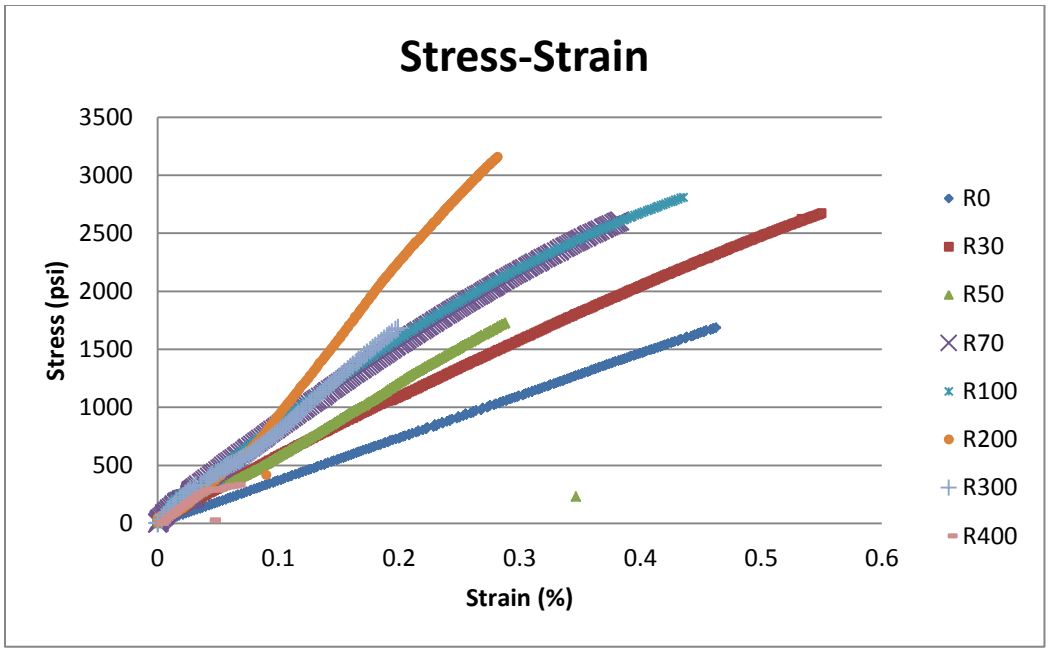

Figure 43: Comparison of stress-strain curve for all specimens (specimen No 1 for all specimens)

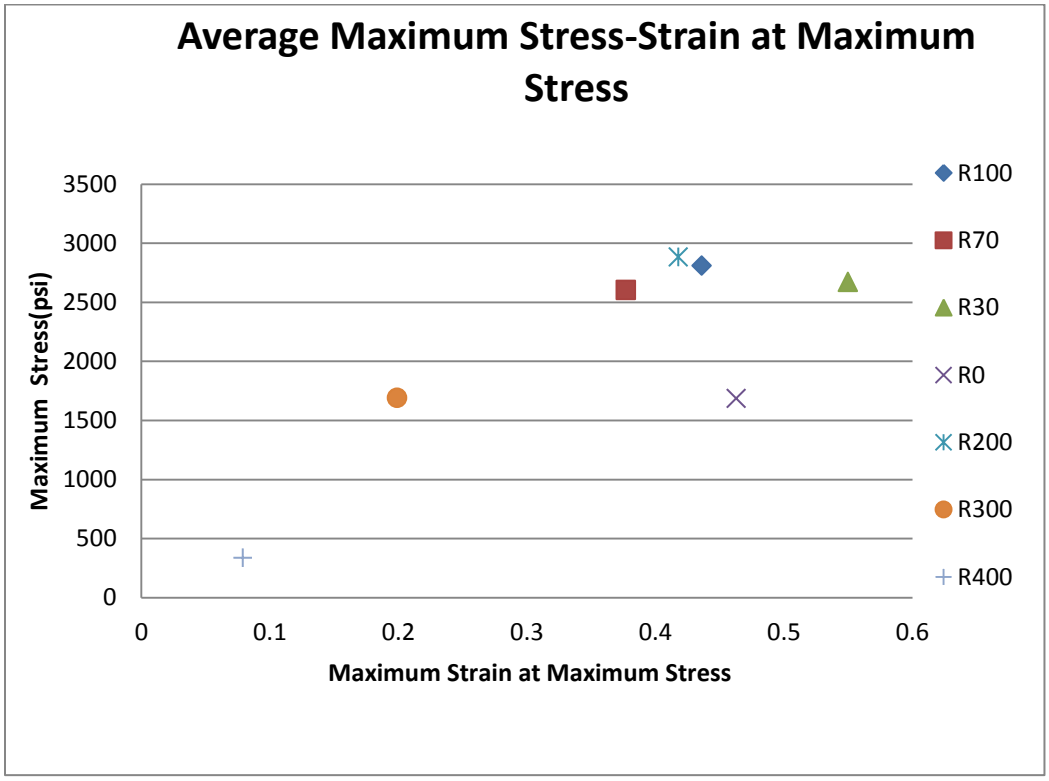

Figure 44: Maximum stress vs. strain at maximum stress, for all specimens.

5.4 Pendulum Impact Testing

Pendulum impact tests for specimens R0, R70, and R100 were conducted. Results of all tests are shown in Table 9.

Table 10 reports the average of the three measured energy parameters for each specimen type. It is desirable for the materials to have higher impact energy values as this indicates higher toughness and energy-absorption capability.

Table 9: The variation of impact energy and strength during pendulum impact tests.

Sample ID	wt%	Depth d(m)	Width w(m)	Impact Energy(J)	Impact Energy per Unit Area (kJ/M^2)	Impact Energy per Unit Length (kJ/m)
R0-1	0	0.0125	0.0109	0.0733	0.534	6.69
R0-2	0	0.0124	0.0109	0.0805	0.587	7.35
R0-3	0	0.0125	0.0109	0.0749	0.547	6.85
R70-1	41.2	0.0126	0.0108	0.0933	0.679	8.55
R70-2	41.2	0.0124	0.0109	0.0910	0.667	8.13
R70-3	41.2	0.0126	0.0109	0.0927	0.6753	8.51
R100-1	50	0.0126	0.0109	0.1089	0.7885	9.97
R100-2	50	0.0124	0.0109	0.0977	0.7184	8.94
R100-3	50	0.0124	0.0109	0.0772	0.5673	7.06

Table 10: The average variation of impact energy and strength during pendulum impact tests.

Sample ID	wt% Gypsum	Depth d (m)	Width w (m)	Impact Energy (J)	Impact Energy per Unit Area (kJ/M^2	Impact Energy per Unit Length (kJ/m)
R0	0.0	0.01251	0.01096	0.076	0.556	6.963
R70	41.2	0.01260	0.01091	0.092	0.6784	8.40
R100	50.0	0.01265	0.01092	0.103	0.753	9.455

Figure 45 shows the average impact energy as a function of FGD gypsum content (in percent). It is clear from the results shown in Figure 45 that the amount of FGD gypsum is an important factor in the impact energy that is achievable. The experimental data indicate that the impact energy increases with increasing FGD gypsum.

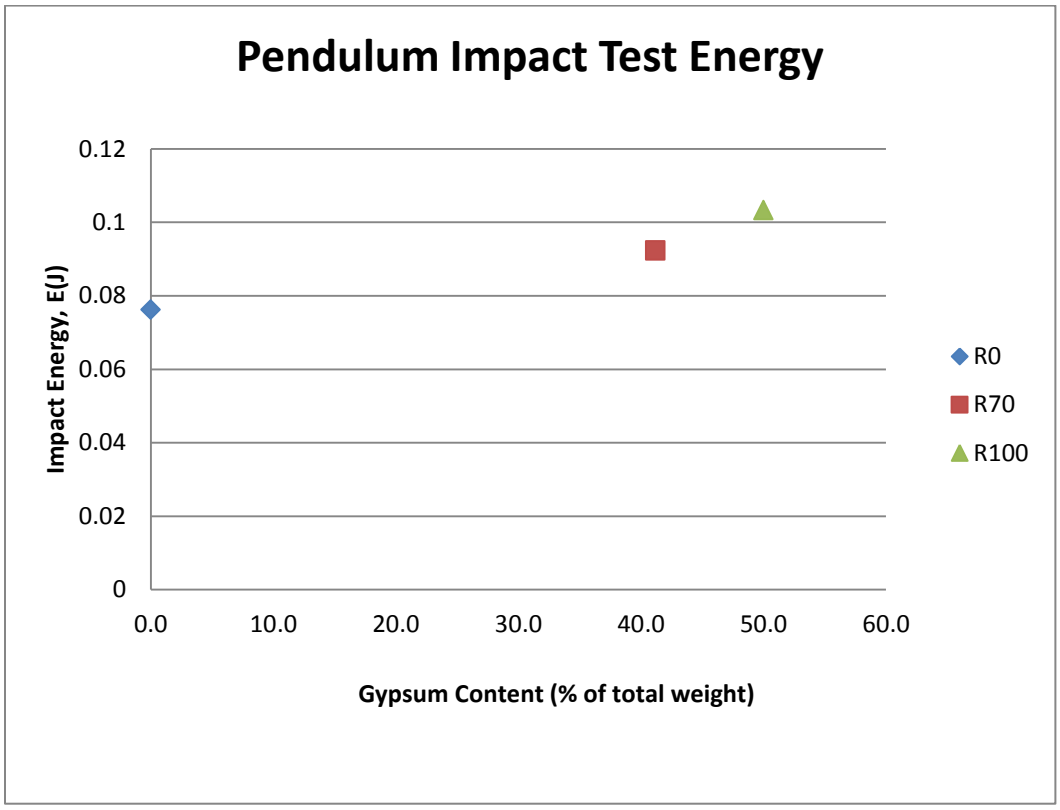

Figure 45: Impact energy increases with weight percent of gypsum.

Results from the pendulum impact test showed that R100 had the highest impact energy among the specimens tested. For the R100 specimen, the average impact energy was higher than the baseline R0 specimen by 35.5%.

5.5 TGA Tests

Figure 46 and Figure 47 show the results of TGA tests for FGD gypsum as well as R0, R40, R70, R100, and R300 materials. All except R300 were tested in air, while R300 was in tested in both air and argon gas. The results are plotted with the x-axis representing temperature and the y-axis representing weight percent of the total mass. TGA tests showed that the R0 specimen rapidly decomposed at about 400°C. As can be seen in Figure 46 for specimen R70, the water loss from hydrated gypsum occurs at approximately 150 °C. The pure FGD gypsum sample shows a 20% mass loss at approximately 150 °C, corresponding to the loss of water from the calcium sulfate dihydrate ($CaSO_4 \bullet 2\ H_20$). As the FGD gypsum content increases, there is less mass reduction at 150 °C, and a significant proportion of the mass is retained up to approximately 800 °C. For the R70 specimen, approximately 40% of the material remained between 400 °C and 700 °C. At 800 °C, roughly 5% of the R0 specimen remained, while 20% of the R30 and 30% of the R70 materials were retained.

Figure 47 similarly shows that the weight loss (mainly water) for R100, R300, and R100 in argon occurs at about 150°C, and the weight loss from decomposition of polymer occurs at about 400 °C. The R100 samples decomposed at slightly higher temperatures in argon than in air. A significant fraction of R300 (approximately 60%) is retained at temperatures up to 1100°C.

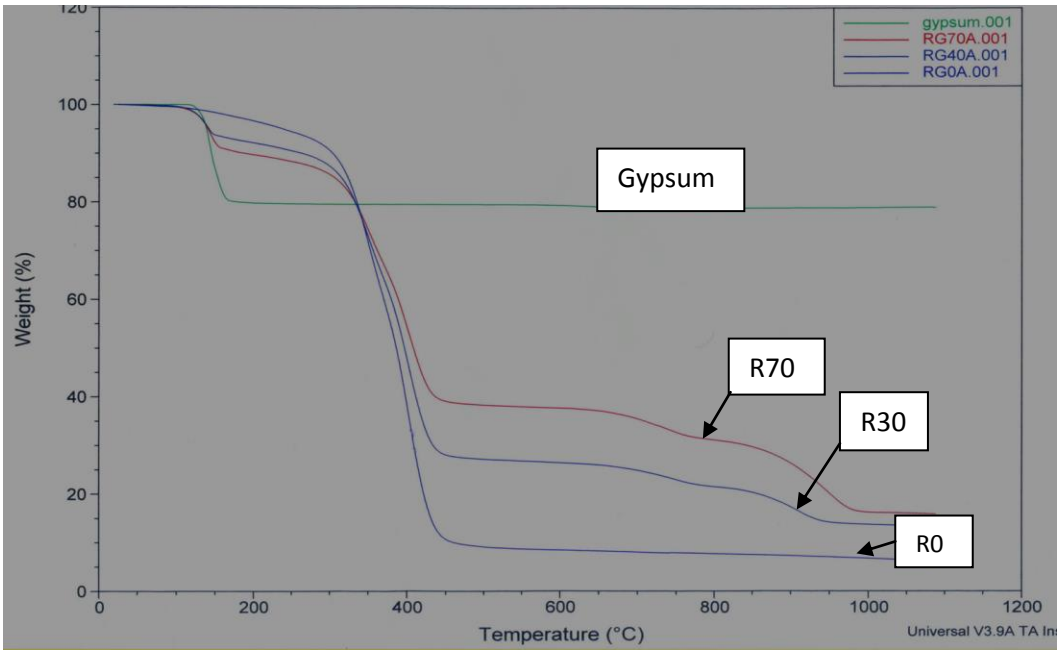

Figure 46: TGA analysis for gypsum, R0, R40, and R70 in air.

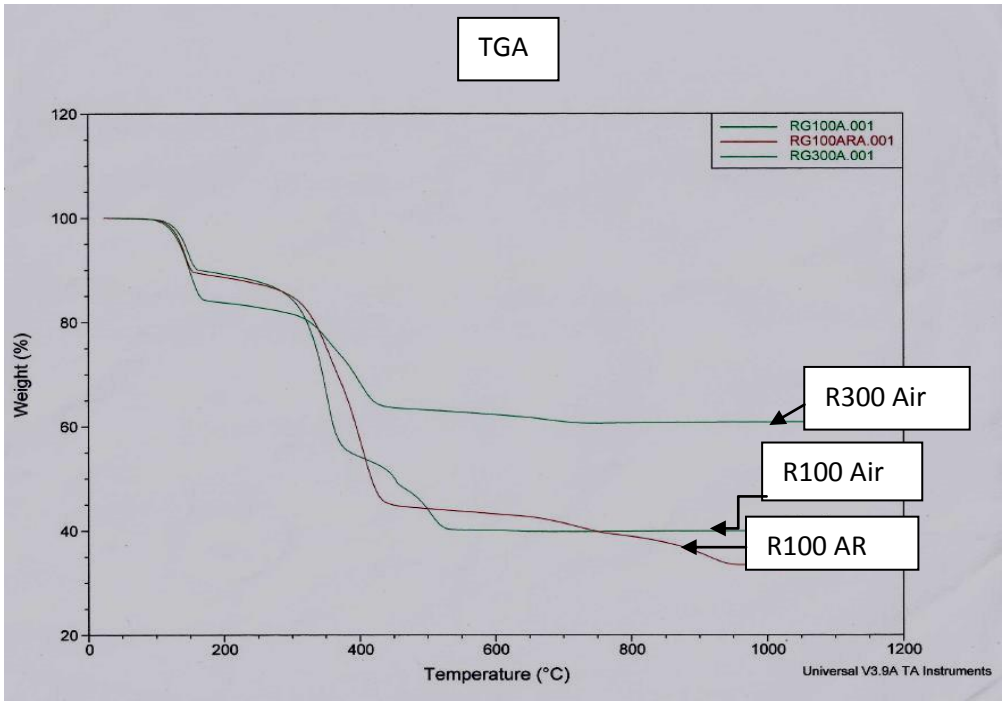

Figure 47: TGA test results for R300 in air, R100 in air, and R100 in Argon.

Figure 48 shows the derivative of TGA results (DTG) for R0, R40, and R70 specimens. The resin is seen to decompose at around 400 °C, and there is further decomposition of gypsum around 750 °C and 950 °C. Unlike R40 and R70, the R0 specimen did not have a DTG peak at 150 °C.

Figure 49 shows that the percentage weight remaining at 700-1100°C for the R300 specimen is about 62%, compared to 80% for the FGD gypsum (Figure 46). The first peak between 150-200 °C is due to water loss from the gypsum phase, and the second and third peaks are due to the pyrolysis during rupture of polymer chains [28].

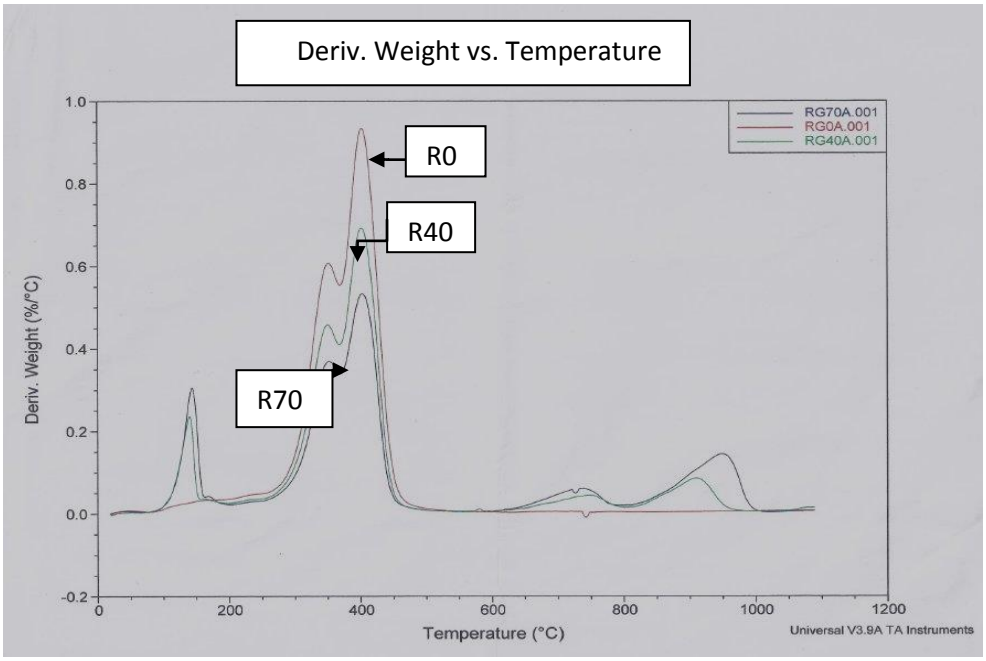

Figure 48: Derivative of weight vs. Temperature (DTG) for R0, R40, and R70.

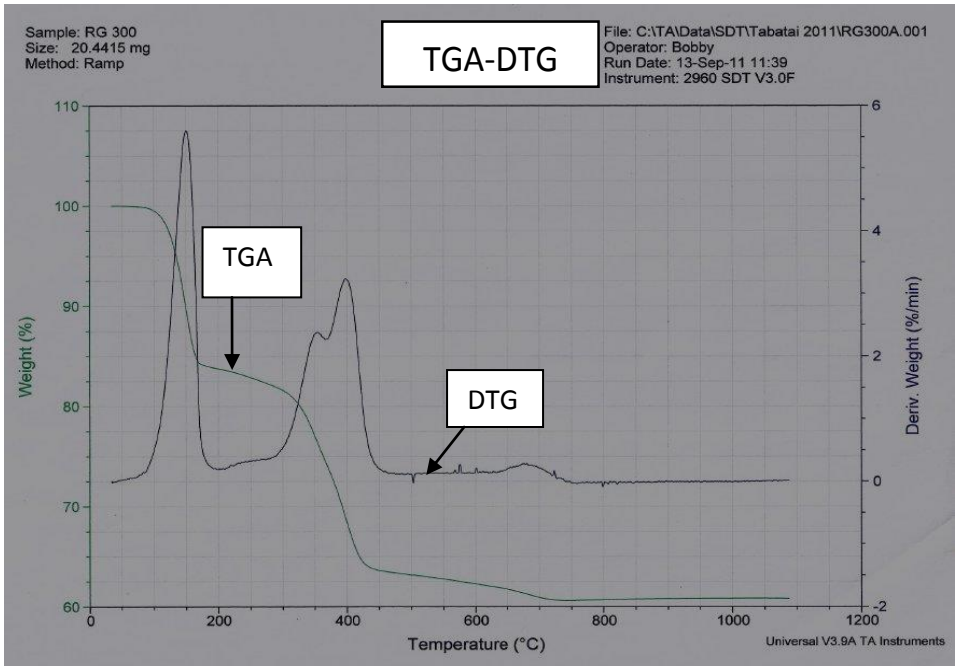

Figure 49: TGA/ DTG for specimen R300.

It would be beneficial to compare FGD gypsum results with other fire-resistant polymers. Figure 50 shows that the percentage weight remaining at 800-1000°C for the PHA-3 and PHA-5 is about 40%. This is comparable to the R100 test that showed 40% remaining at 1100°C (Figure 47) [27].

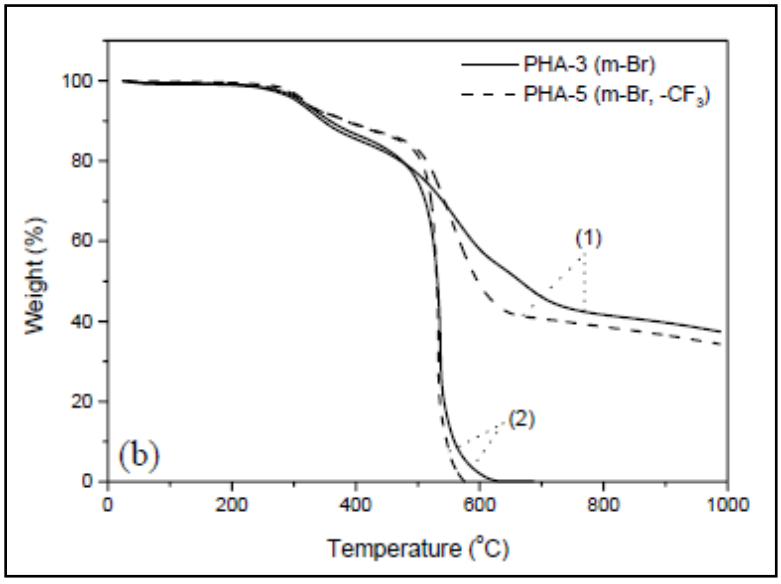

Figure 50: TGA of PHA-3 and PHA-5 samples [27].

Figure 51 shows that the percentage weight remaining at 950-1100°C for the R100 specimen is about 34%, compared to 80% for the FGD gypsum (Figure 46). The first peak around 150 °C is due to water loss from the gypsum phase, and the second peak is due to decomposition of polymer [28].

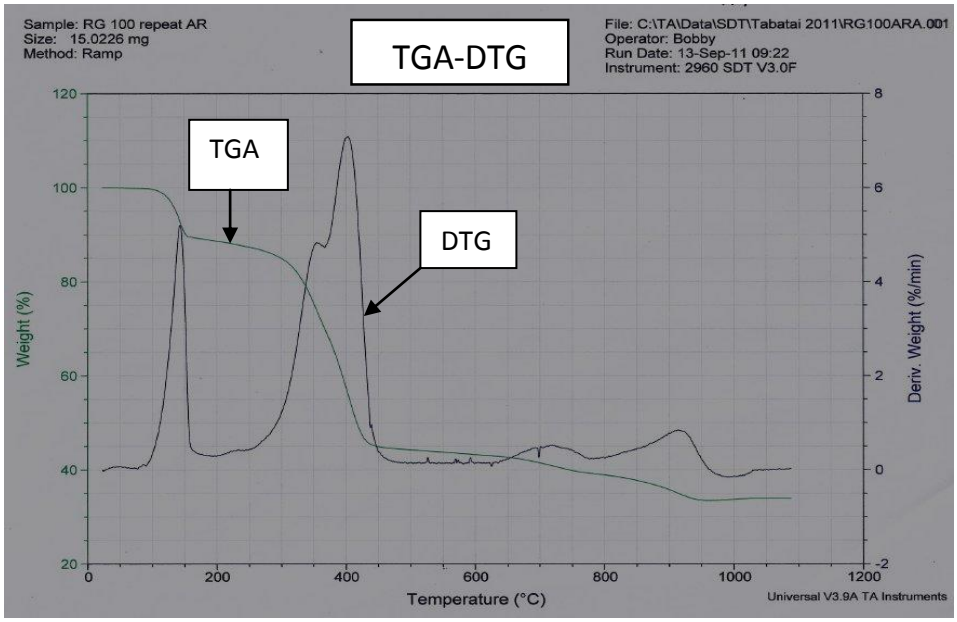

Figure 51: TGA/DTA for Specimen R100.

Figure 52 shows two subsequent DTG results for the R300 material. During the first test, the material undergoes dehydration with a corresponding spike at around 150°C. When the same specimen was reheated, there was no spike, demonstrating that the specimen had been fully dehydrated in the first cycle of heating.

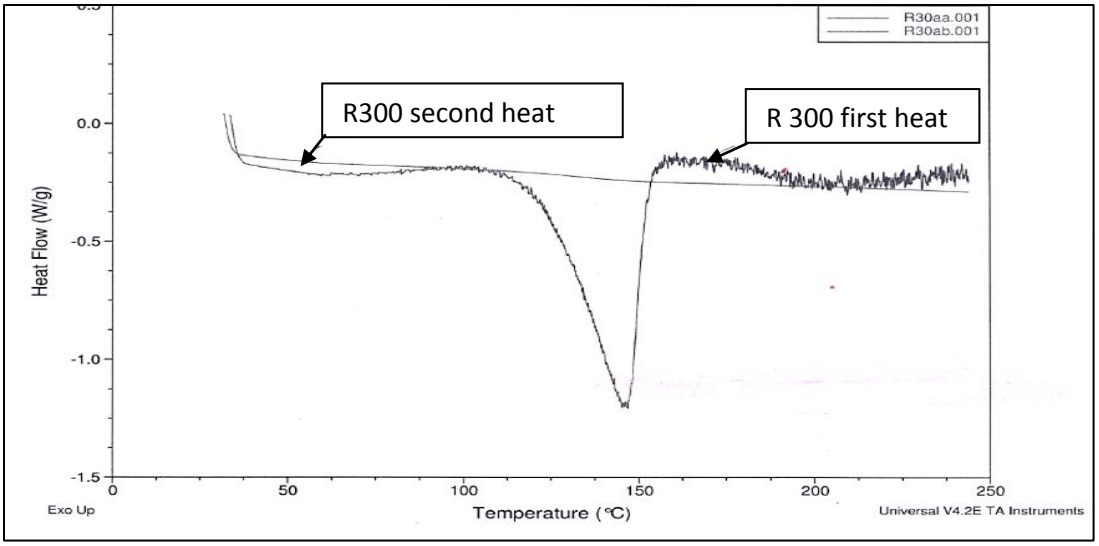

Figure 52: Performing repeated DTG on R300 specimen.

5.6 SEM Tests:

Using SEM, high definition images were obtained from fractured tensile test specimen cross sections to observe patterns in the nature of the fractures. In addition, SEM images of the FGD gypsum itself were obtained. In Figure 53 through Figure 56, the FGD gypsum particles can be seen with different magnifications. Typical FGD gypsum particle sizes are on the order of 30-80 microns.

Figure 59 through Figure 68 display the SEM images of R0, R70, R100, and R300 fracture surfaces at mangifications 1000x, 2000x, and 3000x. The fracture surface for R0 is displayed in Figure 57, Figure 61, and Figure 65, which show a relatively smooth fracture surface. Furthermore, in the other SEM images from Figure 59 through Figure 68, fracture is seen occurring along the jagged gypsum-resin interfaces. In the

FGD gypsum-modified composites, the cumulative crack propagation length is increased by the gypsum particles embedded within the resin because of the jagged interface.

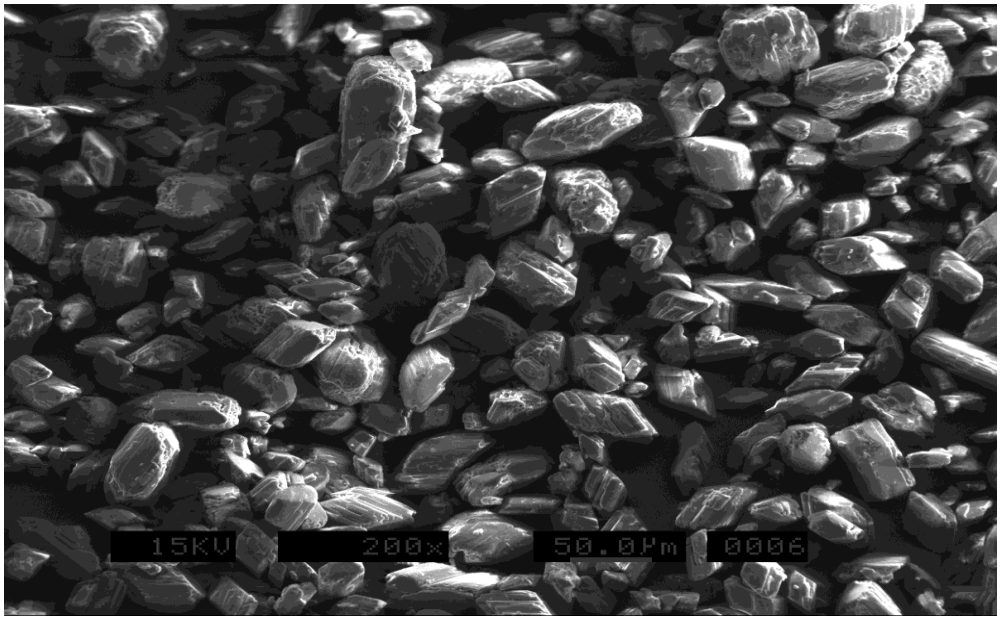

Figure 53: SEM image of FGD gypsum with magnification of 200x.

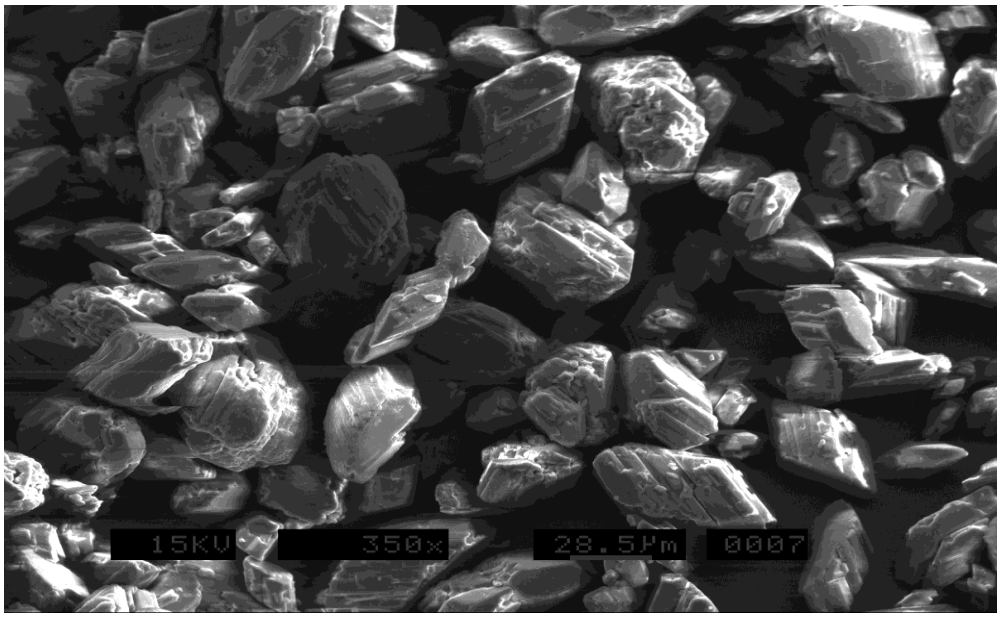

Figure 54: SEM image of FGD gypsum with magnification of 350x.

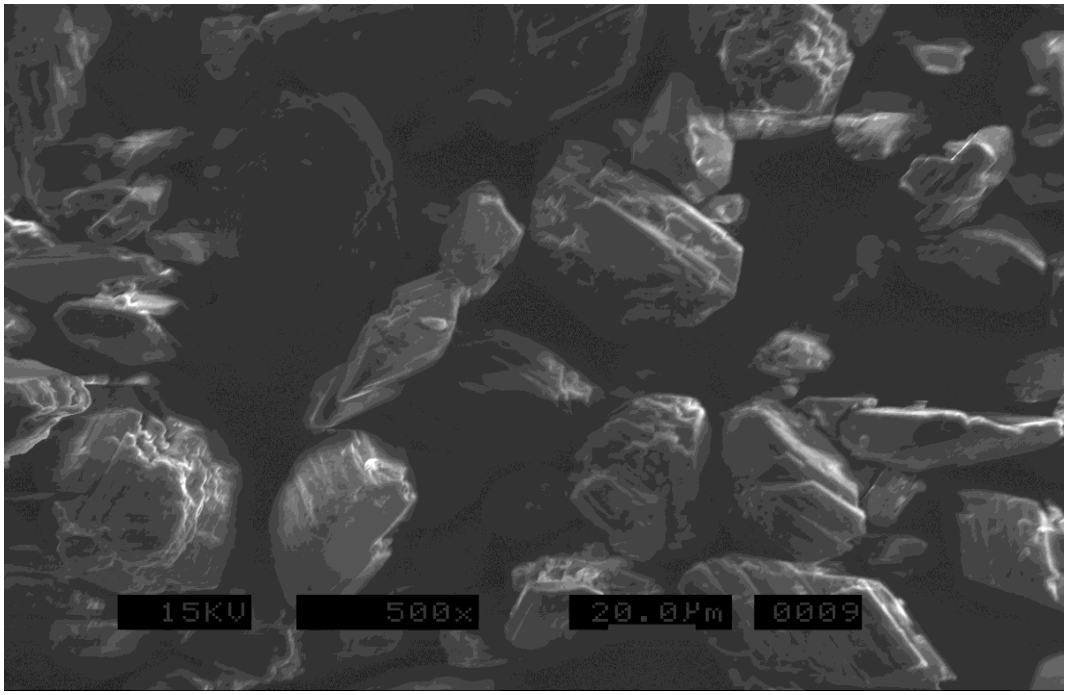

Figure 55: SEM image of FGD gypsum with magnification of 500x.

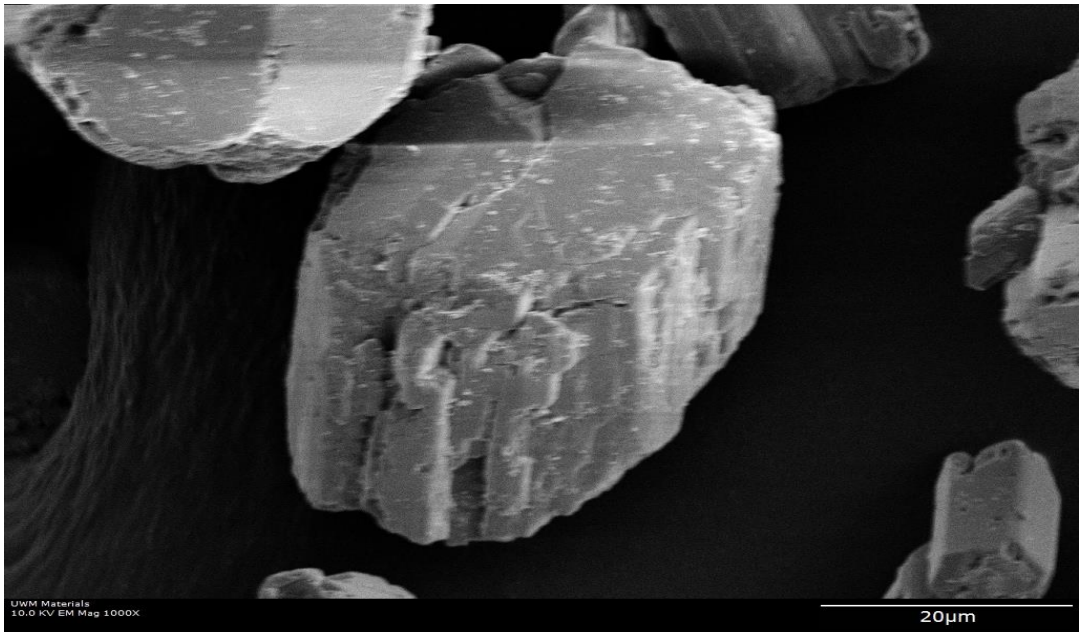

Figure 56: SEM image of FGD gypsum with magnification of 1000x.

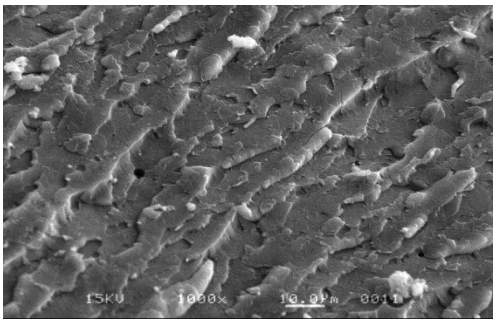

Figure 57: SEM image of fracture surface in tensile specimen R0 (resin polyester) magnification 1000x.

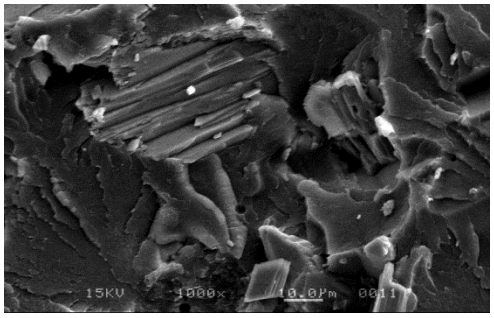

Figure 59: SEM image of fracture surface in tensile specimen R70 magnification 1000x.

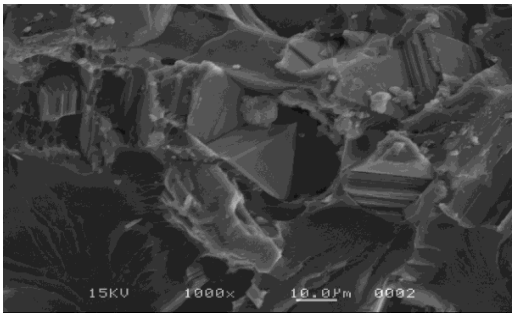

Figure 58: SEM image of fracture surface in tensile specimen R100 magnification 1000x.

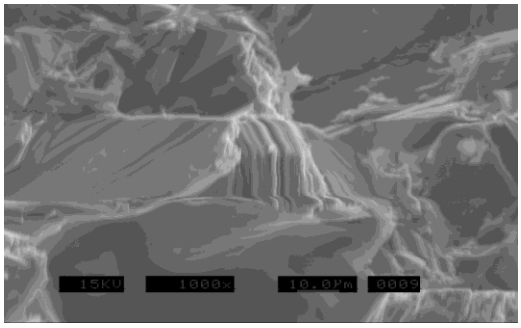

Figure 60: SEM image of fracture surface in tensile specimen R300 magnification 1000x.

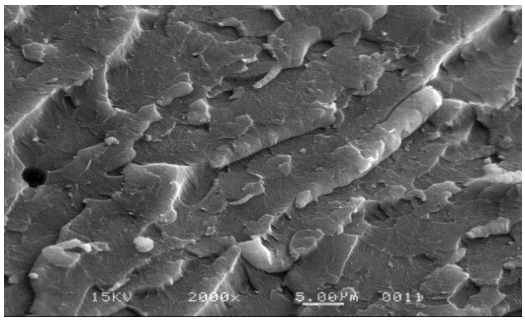

Figure 61: SEM image of fracture surface in tensile specimen R0 (resin polyester) magnification 2000x.

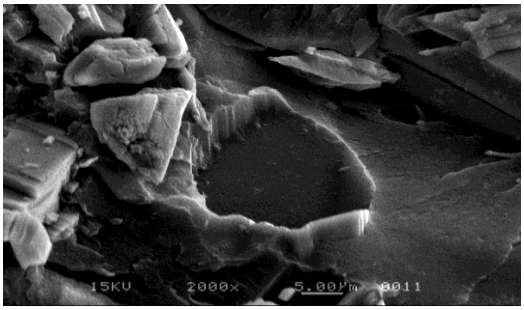

Figure 62: SEM image of fracture surface in tensile specimen R70 magnification 2000x.

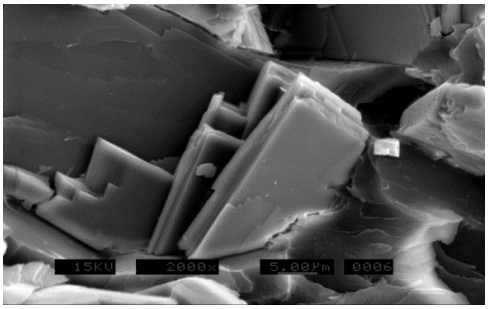

Figure 63: SEM image of fracture surface in tensile specimen R100 magnification 2000x.

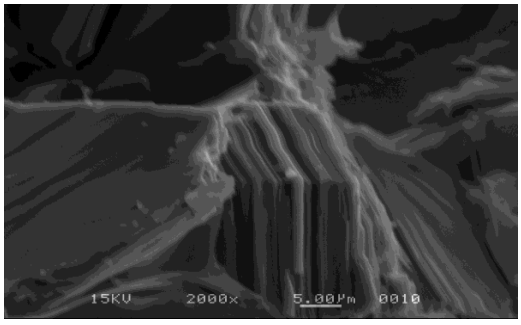

Figure 64: SEM image of fracture surface in tensile specimen R300 magnification 2000x.

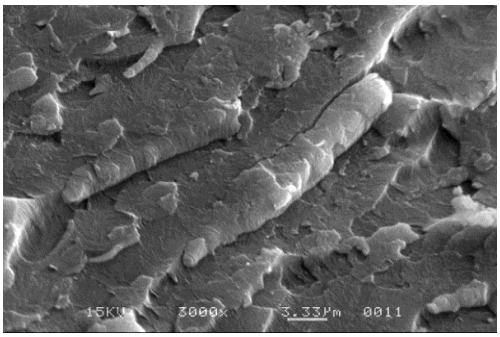

Figure 65: SEM image of fracture surface in tensile specimen R0 (resin polyester) magnification 3000x.

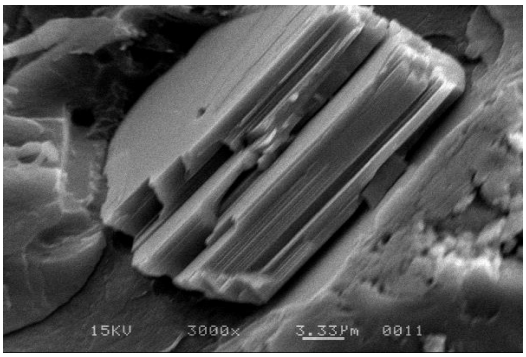

Figure 66: SEM image of fracture surface in tensile specimen R70 magnification 3000x.

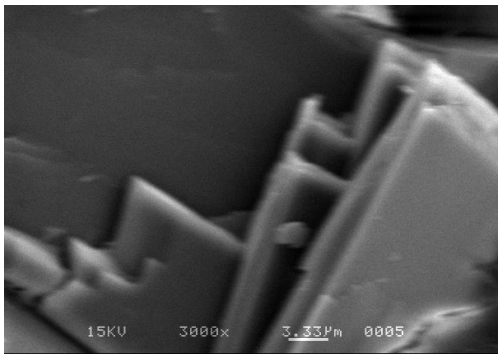

Figure 67: SEM image of fracture surface in tensile specimen R100 magnification 3000x.

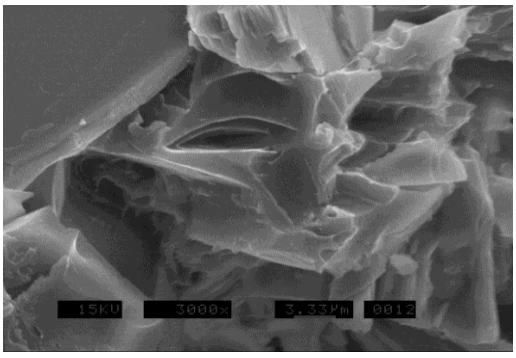

Figure 68: SEM image of fracture surface in tensile specimen R300 magnification 3000x.

6. Conclusions

The results of the compression test indicate that there is an overall reduction in strength as FGD gypsum content increases. In all FGD gypsum-resin compression tests, the color of the material changed from brown to beige just before failure. Tensile strength tests showed increases in tensile strength (up to R100), modulus of elasticity (up to R200), and area under stress-strain curve (up to R100) as FGD gypsum content increased. Open flame tests showed that an effective protective layer of FGD gypsum can form on the surface of the composite such that the interior materials are shielded from fire. The experimental data from the pendulum impact tests indicate that the impact energy increases with the increasing gypsum content up through R100. Composites with FGD gypsum contents higher than R100 were not tested in the pendulum impact tests.

TGA results showed that the thermal decomposition of unmodified resin occurs at around 400 °C. However, TGA results showed that the FGD gypsum composites retain a significant fraction of mass up to 800 °C or higher.

Using SEM, high definition images were obtained of fractured cross sections to observe patterns in the nature of the fractures. Examination of the fracture surfaces showed that the fracture plane follows the resin-gypsum interface. In the R0 specimen, there is a flat (brittle) fracture surface. However, in the R70, R100, and R300 specimens, the fracture surface is jagged and follows the FGD gypsum particle surfaces. This more arduous fracture pattern resulted in higher strength and toughness of the composite material.

Overall, the above test program shows that there is potential for development of fire-resistant polymer composites through the high-volume addition of FDG gypsum additive to polyester resins. FGD gypsum can also improve certain mechanical properties of the composite resulting in higher tensile strength, toughness, and stiffness. FGD gypsum contents in the range of 70 to 100 PPH resulted in optimum mechanical properties. Further development and innovation of this approach may have important implications not only in broadening the use polyester resin–FGD gypsum composite in civil and other applications, but also in beneficial utilization of a significant industrial byproduct.

7. Recommendations for Future Work

It is recommended that further testing be conducted to continue to investigate the effects of varying the proportion of FGD gypsum in resin on the composite's workability, consistency, mechanical properties, and high-temperature performance. In future work, additional supplementary cementitious materials such as fly ash (Class F fly ash and Class C fly ash) could be used with polyester and other types of resin together with FGD gypsum. It is recommended that future studies use larger scale tests and also explore the effects of different types of reinforcing fibers.

8. References

1. Isaac M. Daniel, Ori Ishai, (2006), Engineering Mechanics of Composite Materials, Oxford University Press, 2nd edition.
2. Ziqing Yu and Aixi Zhou, (2010) An Integrated Thermomechanical Method for Modeling Fiber Reinforced Polymer Composite Structures in Fire, 19th Analysis & Computation Specialty Conference, 2010 ASCE.
3. Guojian Wang, Yan Huang, Xiang Hu, (2013), Synthesis of a novel phosphorus-containing polymer and its application in amino intumescent fire resistant coating, Progress in Organic Coatings 76 ,2013 188– 193.
4. Gefu Ji, Guoqiang Li, Walid Alaywan, (2013), A new fire resistant FRP for externally bonded concrete repair, Construction and Building Materials 42 201,2013, 87–96.
5. James Giancaspro, M.ASCE; P. N. Balaguru, M.ASCE; (2006) and Richard E. Lyon, Use of Inorganic Polymer to Improve the Fire Response of Balsa Sandwich Structures, J. Mater. Civ. Eng. 2006.18:390-397.
6. H.-T Chiu, S.-H Chiu, R.-E Jeng, J.-S Chung, A study of the combustion and fire-retardance behaviour of unsaturated polyester/phenolic resin blends, Polymer Degradation and Stability, Volume 70, Issue 3, 2000, Pages 505–514.
7. TANG Hao, ZHOU Xiao-bai, LIU Xiao-lu,(2013) Effect of Magnesium Hydroxide on the Flame Retardant Properties of Unsaturated Polyester Resin, Procedia Engineering 52, 2013, 336 – 341.

8. http://www.uscomposites.com/polyesters.html (access on 07/07/13).
9. Wilhelm Neier, Guenter Strehlke "2-Butanone" in Ullmann's Encyclopedia of Industrial Chemistry, Wiley-VCH, Weinheim, (2002).
10. Turner, Charles F.; McCreery, Joseph W. (1981). The Chemistry of Fire and Hazardous Materials. Boston, Massachusetts: Allyn and Bacon, Inc. p. 118. ISBN 0-205-06912-6.
11. Tesarek, P., Drchalova, J., Kolísko, J., Rovnaníková, P., & Černý, R. (2007). Flue gas desulfurization gypsum: Study of basic mechanical, hydric and thermal properties. *Construction and Building Materials, 21*(7), 1500-1509.
12. Clark, R. B., Ritchey, K. D., & Baligar, V. C. (2001). Benefits and constraints for use of FGD products on agricultural land. *Fuel, 80*(6), 821-828.
13. Klein, C., Hurlbut, C. S., & Dana, J. D. (1993). *Manual of mineralogy* (Vol. 527). New York: Wiley.
14. Van Driessche, A. E. S., Benning, L. G., Rodriguez-Blanco, J. D., Ossorio, M., Bots, P., & García-Ruiz, J. M. (2012). The role and implications of bassanite as a stable precursor phase to gypsum precipitation. *Science*, *336*(6077), 69-72.
15. http://www.templeinland.com/buildingproducts/gypsum/certified/rcgypho w.asp (access on 07/05/13).
16. http://www.fgdproducts.org/Presentations_Indy_11_09/Tue_1330_Larrim ore.pdf (access on 07/07/13).

17. http://www.we-energies.com/environmental/gypsum.htm (access on 07/07/13).
18. http://ohioline.osu.edu/anr-fact/0020.html(Access on 07/07/13)
19. Karni, J., & Karni, E. Y. (1995). Gypsum in construction: origin and properties.*Materials and Structures*, *28*(2), 92-100.
20. https://www.deslinc.com/catalog/concrete-testing/3-gang-cube-mold (access on 07/07/13).
21. http://www.clubkitclearcote.com/techdata/TECHDATASHEETCaptains%20Club%20Resin.pdf (access07/17/13)
22. http://www.ele.com/euro/index.php?option=com_content&view=article&id=112&Itemid=170 (access07/10/13)
23. http://projects.olin.edu/revere/Operating%20Instructions/Instron%208200%20Impact%20Tester%20Operating%20Instructions.pdf(access07/10/13)
24. http://www.perkinelmer.com/CMSResources/Images/44-74556GDE_TGABeginnersGuide.pdf(access07/17/13)
25. Arikan M., and Sobolev K., (2002), The Optimization of a Gypsum-Based Composite Material. CEMENT AND CONCRETE RESEARCH, Vol. 32, No. 11, 2002, pp. 1725-1728.
26. Seyedmohammad S. Shams, Rani F. El-Hajjar, (2013), Overlay patch repair of scratch damage in carbon fiber/epoxy laminated composites, Composites: Part A 49, 148–156.
27. Zhang, H. (2004). Fire-safe polymers and polymer composites. U.S. Department of Transportation, Federal Aviation Administration, Polymer

Science and Engineering University of Massachusetts Amhurst, MA 01003, Composites.

28. Motta, Fabiana V., Ana Paula A. Marques, Carlos A. Paskocimas, Mauricio RD Bomio, Amélia SF Santos, Edson R. Leite, José A. Varela, and Elson Longo. "Synthesis of Ba1-xCaxTiO3 by Complex Polymerization Method (CPM)." (2012).
29. Crompton, T.R. (2012). Physical Testing of Plastics. Smithers Rapra Technology.

APPENDIX: PENDULUM IMPACT TEST RESULTS

Gypsum – Resin Test Data

Using Pendulum Impact Machine

Gypsum (grams)	Resin (grams)	Fraction (G/R)x100
0	125	0

Test Performed By: M.J

Specimen Number: 1

Date of Test: 11/16/11

File Name: R0 - 1

Potential Pendulum Energy: 2.1702 J

Impact Energy: 0.0733 J

Strength 1: 0.534 KJ/m^2

Strength 2: 6.69115 J/m

Measured Cross Section:

Table 11: R0 - 1 Pendulum Impact Test Results

Measurement	Depth (in)	Width (in)	Length (in)
1	.489	.429	
2	.493	.431	
3	.494	.435	
Average	.492	.431	2.523
	Area	.212 in^2	

Gypsum – Resin Test Data

Using Pendulum Impact Machine

Gypsum (grams)	Resin (grams)	Fraction (G/R)x100
0	125	0

Test Performed By: M.J

Specimen Number: 2

Date of Test: 11/16/11

File Name: R0 - 2

Potential Pendulum Energy: 2.1702 J

Impact Energy: 0.0805 J

Strength 1: 0.58738 KJ/m^2

Strength 2: 7.34820 J/m

Measured Cross Section:

Table 12: R0 - 2 Pendulum Impact Test Results

Measurement	Depth (in)	Width (in)	Length (in)
1	.488	.429	
2	.494	.432	
3	.494	.434	
Average	.492	.431	2.520
	Area	.212 in^2	

Gypsum – Resin Test Data

Using Pendulum Impact Machine

Gypsum (grams)	Resin (grams)	Fraction (G/R)x100
0	125	0

Test Performed By: M.J

Specimen Number: 3

Date of Test: 11/16/11

File Name: R0 - 3

Potential Pendulum Energy: 2.1702 J

Impact Energy: 0.0749 J

Strength 1: 0.54747 KJ/m^2

Strength 2: 6.84890 J/m

Measured Cross Section:

Table 13: R0 - 3 Pendulum Impact Test Results

Measurement	Depth (in)	Width (in)	Length (in)
1	.491	.432	
2	.495	.431	
3	.494	.431	
Average	.493	.431	2.516
	Area	.212 in^2	

Gypsum – Resin Test Data

Using Pendulum Impact Machine

Gypsum (grams)	Resin (grams)	Fraction (G/R)x100
87.5	125	70

Test Performed By: M.J

Specimen Number: 4

Date of Test: 11/16/11

File Name: R70 - 1

Potential Pendulum Energy: 2.1702 J

Impact Energy: 0.0933 J

Strength 1: 0.67880 KJ/m^2

Strength 2: 8.55294 J/m

Measured Cross Section:

Table 14: R70 - 1 Pendulum Impact Test Results

Measurement	Depth (in)	Width (in)	Length (in)
1	.498	.428	
2	.496	.429	
3	.494	.430	
Average	.496	.429	2.532
	Area	.212 in^2	

Gypsum – Resin Test Data

Using Pendulum Impact Machine

Gypsum (grams)	Resin (grams)	Fraction (G/R)x100
87.5	125	70

Test Performed By: M.J

Specimen Number: 5

Date of Test: 11/16/11

File Name: R70 - 2

Potential Pendulum Energy: 2.1702 J

Impact Energy: 0.0910 J

Strength 1: 0.66863 KJ/m^2

Strength 2: 8.1348 J/m

Measured Cross Section:

Table 15: R70 - 2 Pendulum Impact Test Results

Measurement	Depth (in)	Width (in)	Length (in)
1	.494	.431	
2	.491	.431	
3	.487	.431	
Average	.490	.431	2.522
	Area	.211 in^2	

Gypsum – Resin Test Data

Using Pendulum Impact Machine

Gypsum (grams)	Resin (grams)	Fraction (G/R)x100
87.5	125	70

Test Performed By: M.J

Specimen Number: 6

Date of Test: 11/16/11

File Name: R70 - 3

Potential Pendulum Energy: 2.1702 J

Impact Energy: 0.0927 J

Strength 1: 0.6753 KJ/m^2

Strength 2: 8.50974 J/m

Measured Cross Section:

Table 16: R70 - 3 Pendulum Impact Test Results

Measurement	Depth (in)	Width (in)	Length (in)
1	.496	.430	
2	.496	.430	
3	.498	.427	
Average	.496	.429	2.520
	Area	.213 in^2	

Gypsum – Resin Test Data

Using Pendulum Impact Machine

Gypsum (grams)	Resin (grams)	Fraction (G/R)x100
125	125	1

Test Performed By: M.J

Specimen Number: 7

Date of Test: 11/16/11

File Name: R100 - 1

Potential Pendulum Energy: 2.1702 J

Impact Energy: 0.1089 J

Strength 1: 0.78853 KJ/m^2

Strength 2: 9.97499 J/m

Measured Cross Section:

Table 17: R100 - 1 Pendulum Impact Test Results

Measurement	Depth (in)	Width (in)	Length (in)
1	.497	.430	
2	.498	.430	
3	.498	.430	
Average	.498	.430	2.519
	Area	.214 in^2	

Gypsum – Resin Test Data

Using Pendulum Impact Machine

Gypsum (grams)	Resin (grams)	Fraction (G/R)x100
125	125	1

Test Performed By: M.J

Specimen Number: 8

Date of Test: 11/16/11

File Name: R100 - 2

Potential Pendulum Energy: 2.1702 J

Impact Energy: 0.09777 J

Strength 1: 0.71838 KJ/m^2

Strength 2: 8.93668 J/m

Measured Cross Section:

Table 18: R100 - 2 Pendulum Impact Test Results

Measurement	Depth (in)	Width (in)	Length (in)
1	.488	.428	
2	.491	.432	
3	.493	.430	
Average	.490	.430	2.520
	Area	.210 in^2	

Gypsum – Resin Test Data

Using Pendulum Impact Machine

Gypsum (grams)	Resin (grams)	Fraction (G/R)x100
0	125	0

Test Performed By: M.J

Specimen Number: 9

Date of Test: 11/16/11

File Name: R0 - 3
Potential Pendulum Energy: 2.1702 J

Impact Energy: 0.0772 J

Strength 1: 0.56733 KJ/m^2

Strength 2: 7.05765 J/m

Measured Cross Section:

Table 19: R100 - 3 Pendulum Impact Test Results

Measurement	Depth (in)	Width (in)	Length (in)
1	.496	.430	
2	.486	.430	
3	.482	.430	
Average	.490	.430	2.52
	Area	.210 in^2	